MASTHING: a process-based model of mast seeding in European beech

Simone Bregaglio[1,*], Sofia Bajocco[1], Carlotta Ferrara[2], Michał Bogdziewicz[3], Andrew Hacket-Pain[4], Francesco Chianucci[2]

[1] Council for Agricultural Research and Economics (CREA) – GeoModel lab – Research Centre for Agriculture and Environment, Italy.

[2] Council for Agricultural Research and Economics (CREA) – Research Centre for Forestry and Wood, Italy.

[3] Forest Biology Centre, Institute of Environmental Biology, Faculty of Biology, Adam Mickiewicz University, Uniwersytetu Poznańskiego 6, 61-614 Poznań, Poland.

[4] Department of Geography and Planning, School of Environmental Sciences, University of Liverpool, Liverpool, United Kingdom.

*corresponding author: simoneugomaria.bregaglio@crea.gov.it

Summary

Masting, the synchronised interannual variation in seed production, shapes forest regeneration and many ecosystem processes, yet process-based models remain underdeveloped. Here we introduce MASTHING (MASting THeory modellING), an individual-tree model coupling phenology, carbon gain, resource storage, temperature cues, and environmental vetoes on reproduction. We parameterised MASTHING for European beech (*Fagus sylvatica* L.) using 43 years of data from 100 trees across 11 sites in England to test alternative hypotheses about masting mechanisms. Three formulations were compared: resource budget only (RB), and extensions with additive (RB+WC) and interactive (RB×WC) temperature cue effects. Performance improved with complexity and was highest when cue sensitivity depended on internal resource status. At the site-year scale, explained variance increased from R^2 = 0.58 (RB) to R^2 = 0.76 (RB×WC), supporting that favourable cues trigger strong reproduction only when sufficient resources have accumulated. The model reproduced mast and failure years, partly captured long-term breakdown in masting intensity under climate warming, and broadly predicted seed production during 2023-2025, although low-seed years were less well predicted. Modelled resource and cue dynamics were sufficient to simulate short-term variation and progressive weakening of reproductive pulses. MASTHING provides a platform for testing masting hypotheses, evaluating climate change impacts, and supporting operational seed forecasting.

Keywords: climate change, masting, fecundity, forest resilience, tree demography

1. Introduction

Masting, the synchronized interannual variability in seed production among individuals within a population, is a common reproductive strategy in long-lived plants (Kelly & Sork, 2002; Journé *et*

al., 2023). This variable reproduction enhances reproductive efficiency by reducing seed predation and improving pollination success (Kelly *et al.*, 2001; Rapp *et al.*, 2013; Zwolak *et al.*, 2022). The resulting boom-and-bust dynamics in seed supply have far-reaching implications for food webs, nutrient cycling, and the dynamics of plant and fungal communities, as well as for forest ecosystems and game management (Ostfeld & Keesing, 2000; Bisi *et al.*, 2018 Clark *et al.*, 2019; Pearse *et al.*, 2021; Tattoni *et al.*, 2025). Understanding the mechanisms underlying masting is therefore essential for predicting changes in plant populations and ecosystem functioning (Hacket-Pain & Bogdziewicz, 2021) and for providing short-term forecasts of seed production to support decision-making (Elliott & Kemp, 2016; Journé *et al.*, 2023). These needs are becoming particularly urgent as climate change alters masting patterns, with large consequences for seed availability (Bogdziewicz *et al.*, 2023; Jantzen *et al.*, 2026). At the same time, demand for reliable short-term forecasting is increasing as seed supply for ecological restoration becomes a policy priority (Pearse *et al.*, 2021; Journé *et al.*, 2023; Oberklammer *et al.*, 2026). For example, the European Union's Biodiversity Strategy for 2030 and the proposed EU Nature Restoration Law emphasise large-scale ecosystem restoration, which requires a dependable supply of seeds. Accurate forecasting is therefore essential to ensure adequate seed availability for restoration projects.

Building on this growing interest, recent decades have brought significant progress in understanding the processes driving interannual variation and synchrony in seed production (Crone & Rapp, 2014; Pearse *et al.*, 2016; Bogdziewicz *et al.*, 2024; Satake & Journé, 2026). These advances open the way to models capable of reproducing masting dynamics, enabling near-term forecasting and assessing climate change impacts on plant reproduction. However, most existing approaches remain primarily statistical (Journé *et al.*, 2023; Wion *et al.*, 2025; Hirsch *et al.*, 2025; Oberklammer *et al.*, 2026). Process-based models offer a valuable alternative, as they explicitly represent underlying biophysical mechanisms rather than relying on empirical relationships (Asse *et al.*, 2020; Mäkelä *et al.*, 2000). This mechanistic foundation can improve predictive skill, especially under changing environmental conditions, making such models powerful tools for ecological forecasting and management (Briscoe *et al.*, 2022). Moreover, because masting operates over multiple years and is difficult to manipulate experimentally (Bogdziewicz *et al.*, 2020a), process-based models provide a means to test hypotheses and simulate scenarios that are otherwise impractical in field studies (Végh & Kato, 2024).

Various models have been developed to explain masting, including those based on resource budgets, weather cues, and resource-limited floral induction (Isagi *et al.*, 1997; Kelly *et al.*, 2013; Monks *et al.*, 2016; Pearse *et al.*, 2016). Rather than acting independently, the General Model of Masting (Bogdziewicz *et al.*, 2024) suggests that these mechanisms jointly regulate the transition to

flowering to fruiting, with their relative importance varying across species. Resource budget models propose that plants must accumulate sufficient resources before reproduction, often over multiple years (Isagi *et al.*, 1997; Crone & Rapp, 2014), and experimental flower removal confirms that reproduction depletes resources and limits subsequent flowering (Sala *et al.*, 2012; Roncé *et al.*, 2023). In parallel, weather cue models suggest that plants evolved hypersensitivity to environmental variability, triggering large seed crops under favourable conditions such as specific temperature regimes (Janzen, 1971; Kelly *et al.*, 2013; Fernández-Martínez *et al.*, 2017; Yeoh *et al.*, 2017; Bogdziewicz *et al.*, 2020b). Resource-limited floral induction links these mechanisms by proposing that responses to weather cues depend on internal resource status (Monks *et al.*, 2016; Kelly *et al.*, 2025). For example, in *Nothofagus solandri*, nitrogen fertilization removed resource limitation, resulting in a positive relationship between temperature during flower formation and seed production that was absent in non-fertilized control stands (Smaill *et al.*, 2011). Together, these advances provide a solid conceptual basis for process-based models of masting. However, such models remain rare (Vacchiano *et al.*, 2018), and recent developments still require evaluation under changing climatic conditions (Végh & Kato, 2024).

Here, we present MASTHING (MASting Theory modellING), a dynamic simulation model that represents key processes underlying plant reproduction. The model proposes a resource budget framework coupled to plant phenology, where carbon gained through photosynthesis is allocated to reproduction as a function of internal resource status and environmental cues. We parameterised MASTHING for European beech (*Fagus sylvatica*) using 43 years of seed production data (1980–2022) from 100 trees across 11 sites in England (Packham *et al.*, 2008a; Bogdziewicz *et al.*, 2020c), and evaluated its forecasting skill for 2023-2025. Using this framework, we tested whether the proximate mechanisms hypothesised to drive masting in beech can reproduce observed reproductive dynamics. We further investigated whether the model can reproduce the recent breakdown of masting patterns linked to climate warming, characterised by reduced interannual variability and synchrony in seed production (Bogdziewicz *et al.*, 2020c; 2023). This decline has been attributed to more frequent temperature cues, which shorten resource recovery intervals and dampen reproductive responses (Bogdziewicz *et al.*, 2021; Hacket-Pain *et al.*, 2025; Kelly *et al.*, 2025). MASTHING provides a tool to evaluate this hypothesis under changing environmental conditions.

2. Description

2.1. Model overview

MASTHING is a process-based simulation model of individual tree reproductive cycles, derived from the resource-budget theory of Isagi *et al.* (1997) and extended into a process-based framework (Figure 1).

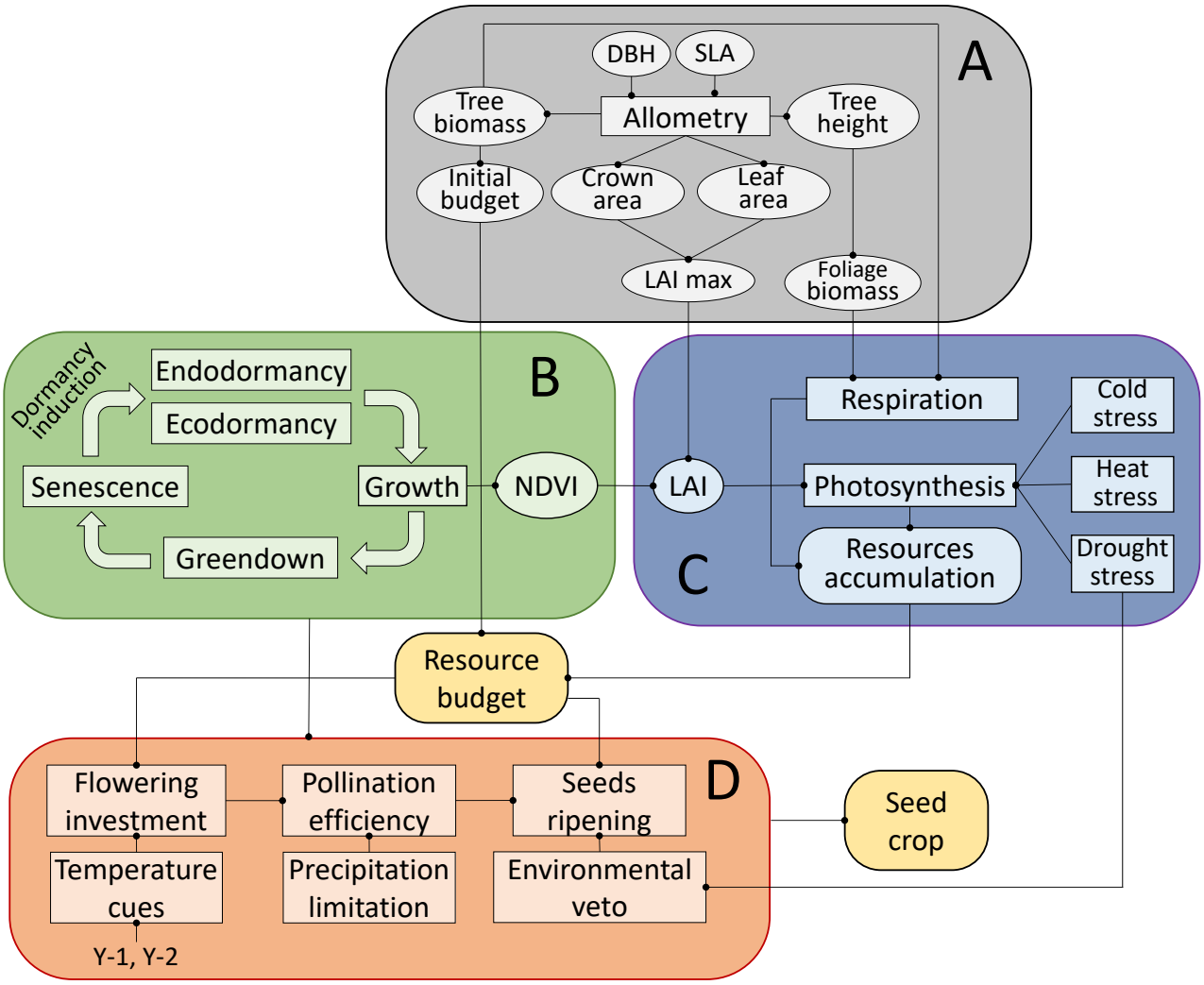

Figure 1. Conceptual diagram of the MASTHING model showing interlinked modules and simulated processes. (A) variables associated with the tree allometry module; (B) phenological processes; (C) processes related to resource accumulation; (D) reproductive allocation. Lines and nodes connections indicate relationships among variables and modules.

The model integrates four coupled modules, i.e., tree allometry, phenology, carbon balance, and reproductive allocation (Figure 1). It initializes an individual European beech tree from allometric relationships based on diameter at breast height (DBH, measured at 1.3 m), used to estimate crown area, tree height, and biomass partitioning among plant compartments (Figure 1A; Bartelink, 1997; Zianis & Mencuccini, 2004). Foliage biomass is converted into leaf area index using specific leaf area (SLA, m^{-2} kg) scaled to crown projection area, yielding maximum leaf area index (LAI_{max}. Figure 1A). Phenological dynamics are simulated using the SWELL model (Bajocco *et al.*, 2025), which describes the transition from dormancy to the growing season and the progression of key phenophases (Figure 1B). The resulting simulated Normalised Difference Vegetation Index (NDVI) is scaled over the growing season (bud burst – leaf fall) and used to derive daily leaf area index (LAI) by proportional scaling to LAI_{max} (Bregaglio *et al.*, 2023). Carbon

assimilation is computed using a light-use efficiency framework (Figure 1C; Monteith, 1972; Medlyn, 1998). Gross primary production is driven by incoming radiation and downregulated by temperature and water stress functions (Maselli *et al.*, 2020; Zhao *et al.*, 2019), while maintenance respiration of woody and foliage tissues is represented using a temperature-dependent Q_{10} formulation (Lin *et al.*, 2012). The daily net carbon balance updates the internal resource budget, which represents the central state variable governing reproduction (Figure 1C). The resource budget accumulates carbon over successive seasons and is evaluated at the end of each year, when it is normalised between a baseline reproduction level (B_{rep}, g C m^{-2}) and a maximum storage capacity (B_{max}, g C m^{-2}) to determine a normalised budget level (BL_t, $\in$ [0, 1]). Reproductive allocation (Figure 1D) links the internal resource budget to seed production through flowering investment, pollination, and seed maturation, all potentially modulated by environmental conditions. A full mathematical description of all model components is given in Supplementary Information S1.

2.1.1. Reproductive allocation, temperature cues and environmental filtering

Reproductive investment is allocated sequentially to flowering and seed production (Figure 2). Flowering represents the initial reproductive cost, subtracted from the internal resource budget, while the subsequent conversion of flowers into seeds depends on pollination success. Environmental conditions can modulate reproductive outcomes at different stages within the growing season (Figure 2A). Precipitation during flowering may reduce pollination efficiency (Sofiev *et al.*, 2013), whereas drought during seed development can limit seed filling, acting as an environmental veto (Figure 2B; Bogdziewicz *et al.*, 2018). Under such conditions, part of the carbon initially allocated to reproduction is not converted into seeds and is retained within the internal resource pool (Figure 2B). This carry-over links successive years, as retained resources contribute to future reproductive potential and interact with prior reproductive costs and lagged climatic forcing (Section 2.1.1; Figure 2C).

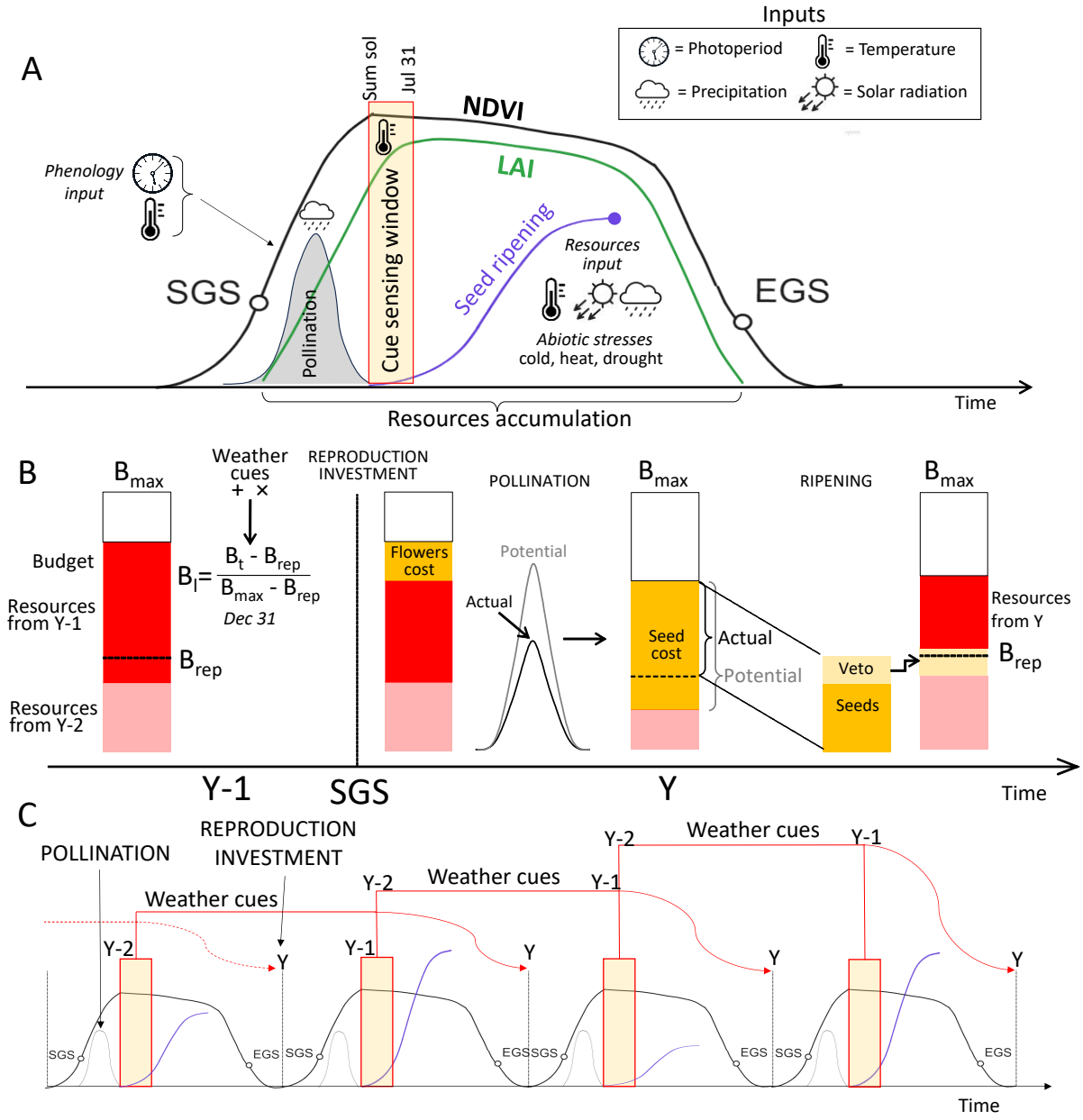

Figure 2. Overview of the MASTHING model across temporal scales. (A) Within-year dynamics linking phenology, canopy development (NDVI = black; LAI = green), environmental forcing, and reproductive timing; the yellow bar indicates the temperature cue sensing window, the grey bell-shaped curve flowering and pollination, and the purple curve seed development; (B) Conceptual representation of reproductive allocation and environmental filtering, where carbon allocated to flowers and seeds may be reduced by pollination failure or drought, with unused resources retained in the internal budget; (C) Multi-year schematic showing how temperature cues from the two preceding years (Y-1 and Y-2; orange bars) contribute to reproductive potential in year Y. Grey lines show flowering, the purple line seed development, and the black line NDVI;

Environmental regulation is introduced through temperature cues derived from conditions during a fixed summer window. Following empirical evidence (Journé *et al.*, 2024), maximum daily temperatures between June 21 and July 31 are aggregated to define an annual flowering cue. To account for lagged responses in masting systems, cue information from the two years preceding

seed production (i.e., Y-1 and Y-2) is retained, combining an activating component from year Y-1 and an inhibitory legacy effect from year Y-2. These components are transformed through sigmoidal response functions and combined into a composite climatic signal (TC_t), scaled between 0 and 1 (Figure S2).

Reproductive allocation depends on both internal resource status and climatic forcing. In the resource-budget-only formulation (RB), allocation is determined solely by the normalised resource level (BL_t). In weather-cue formulations (RB+WC and RB×WC), temperature cues contribute additively to reproductive potential, acting either independently of or interactively with resource availability. In the interactive case (RB×WC), cue sensitivity is modulated by resource availability, producing a resource-gated response. Reproductive investment is computed as a continuous function of these drivers and constrained by the available resource budget:

$$I_{rep} = \min\left(B_t,\ B_{max} \cdot \frac{BL_t + TC_t}{2}\right) \quad [1]$$

where I_{rep} (g C m^{-2}) is reproductive investment, B_t is the current resource budget (g C m^{-2}), and B_{max} is the maximum storage capacity (g C m^{-2}). BL_t represents the normalised resource level, while TC_t the composite temperature cue derived from lagged climatic signals.

2.1.2. Model assumptions and implementation

MASTHING is implemented in C# as a class library coupled with a console application for execution and parameter optimisation, with code available in an open-access repository (Bregaglio et al., 2026; https://github.com/GeoModelLab/MASTHING, DOI: 10.5281/zenodo.19660460). In its current implementation, the resource budget is allocated exclusively to reproduction carbon allocation to other sinks such as growth is not explicitly represented, though the framework can be extended to multiple carbon pools by partitioning the resource budget into parallel compartments. While carbon is not the only resource potentially limiting reproduction, the resource budget used here functions as a proxy for overall physiological readiness, integrating the net carbon balance across the growing season; explicit representation of other nutrient cycles is beyond the current scope (Kabeya, 2021; Végh & Kato, 2024).

2.2. Calibration and evaluation

2.2.1. Input data

Model calibration and evaluation were performed using individual-level observations of beech (*Fagus sylvatica* L.) seed production collected across 11 locations in the UK from 1980 to 2025 (Hacket-Pain *et al.*, 2025; Supplementary Figure S3). Sites span a latitudinal gradient from Woodbury

in the southwest to Benwell in the northeast, covering a range of climatic and edaphic conditions representative of the UK beech distribution. Each site included between 8 and 20 monitored trees (after excluding individuals with fewer than 10 years of observations), with observation periods ranging from 1980 to 2025 across sites (Figure S3). DBH was measured during field sampling, as detailed in Packham *et al.* (2008b) and Bogdziewicz *et al.* (2023). Seed production data from 1980-2022 were used for model calibration and hypothesis testing, while data from 2023–2025 were used to evaluate prospective forecasting performance on out-of-sample years. To parameterise the phenological component of MASTHING, vegetation dynamics were derived from remotely sensed MODIS NDVI imagery at 250 m resolution (8-day maximum value composite; Holben, 1986) over the period 2001-2022, processed using the MODISTools package (Hufkens, 2023). Daily meteorological inputs, including air temperature (°C), precipitation (mm), and incoming radiation (MJ m^{-2} d^{-1}), were obtained for each site from the ERA5 reanalysis dataset (Copernicus Climate Change Service), accessed via Google Earth Engine.

2.2.2. Simulation experiments

A set of simulation experiments was designed to evaluate the relative role of resource dynamics and climatic cues in controlling reproductive investment. Three model formulations were compared: a resource-budget-only model (RB), and two extensions including temperature cues, with additive (RB+WC) and interactive (RB×WC) effects on reproductive allocation (Section 2.1.1.). These formulations represent alternative ecological hypotheses regarding the mechanism underlying mast seeding, in particular the RB×WC formulation consider that sensitivity to climatic cues depends on internal resource status (Kelly *et al.*, 2025). Comparing model performance across formulations therefore constitutes a test of these hypotheses rather than a conventional model selection exercise. Each formulation was evaluated under two contrasting parameterisation strategies. In the first, parameters were calibrated independently for each site (site-specific parameterisation) providing an estimate of maximum attainable model performance. In the second, a single parameter set was estimated jointly across all sites (domain-wide parameterisation) to evaluate model generality across environmental gradients. All simulations were performed at the individual tree level. Outputs were aggregated to the site-year level by computing the mean normalised reproductive investment across all trees within each site and year.

2.2.3. Calibration methodology

Model parameters were derived from a combination of literature sources and data-driven calibration. The majority of parameters were fixed a priori to values reported in the literature, while

a subset for which no reliable species-specific estimates exist was estimated through optimisation (Supplementary Table S1.6). Calibration was performed in two sequential steps. In the first step, the photothermal threshold governing the onset of growth, greendown and senescence phases were optimised against MODIS NDVI time series as the target variable. Optimisation was carried out using a multi-start downhill simplex algorithm minimising the root mean square error (RMSE) between simulated and observed NDVI. To mitigate the risk of equifinality and parameter collinearity, 10 independent optimisation runs were performed, each comprising 10,000 iterations. Model transferability was assessed through a spatial split-sample approach, in which study sites were randomly partitioned into calibration (50%) and validation (50%) subsets. Phenological parameters were then averaged across sites and held fixed in the second. In the second step controlling the reproductive component, five parameters were then optimised (Table S1.6) using the full 1980–2022 observational record, with R^2 between simulated and observed interannual variability in seed production as the objective function. Rather than partitioning the time series into calibration and validation subsets, we used the complete historical record to maximise the ecological signal available for parameter estimation and to ensure that performance differences among the three formulations (RB, RB+WC, RB×WC) reflect mechanistic differences rather than dataset partitioning choices. The prospective forecasting performance of the model was then evaluated on the 2023–2025 data (years not used in any stage of calibration), providing an independent evaluation of the operational prediction skill under real-world conditions.

3. Results

3.1. Model behaviour and emergent dynamics

Before evaluating model performance, we examined the internal dynamics generated by MASTHING to assess whether the model reproduces the characteristic temporal patterns of mast seeding (Figure 3), using the Buckholt site as an example.

Over two consecutive growing seasons (Figure 3A), the model captures the full sequence of phenological and reproductive processes. Pollination efficiency peaked in spring and was sensitive to precipitation-driven vetoes, while resource rate tracked canopy development over the summer months. The resource budget declined progressively as reproductive investment increased, reaching its minimum at the time of seed maturation, before recovering due to carbon assimilation in the last part of autumn. Temperature cues from the preceding two years modulated the magnitude of reproductive investment: the activating signal from Y−1 and the inhibitory legacy from Y−2 combined into a composite cue that differed between 2013 and 2014, generating contrasting seed outputs despite broadly similar seasonal trajectories.

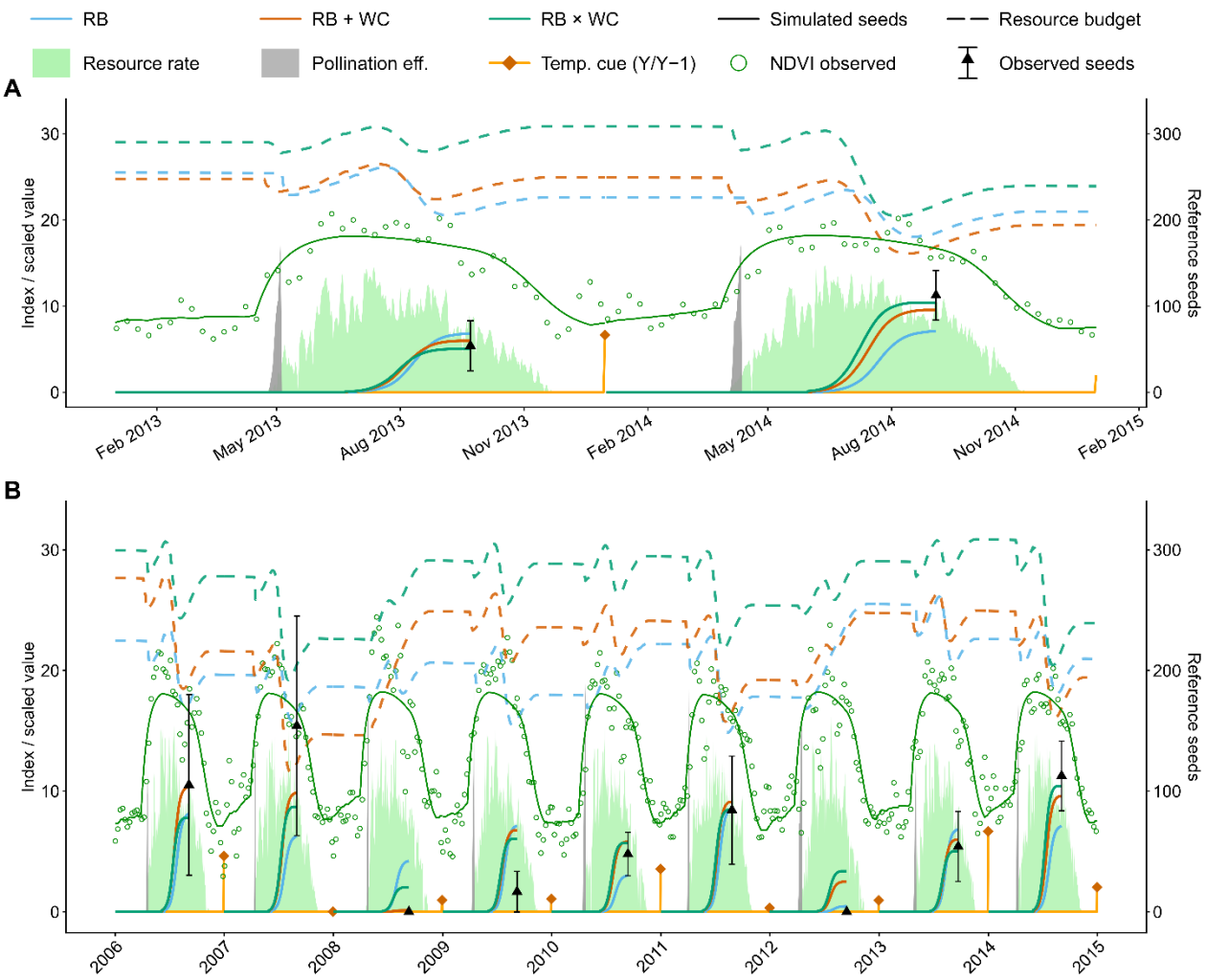

Figure 3. Within- and among-year dynamics simulated by MASTHING for the Buckholt site. (A) Two-year sequence (2013–2014) showing daily resource rate (green area), pollination efficiency (grey area), temperature cues (orange line and diamond, positioned at the last day of year Y-1), observed and simulated NDVI (open grey circles and lines), resource budget (dashed lines), simulated seed production (solid lines), and observed seed count with inter-tree variability (black triangle ± SD). (B) Multi-year simulation (2006–2014) showing the same variables across consecutive growing seasons, illustrating interannual carry-over dynamics in resource budget and reproductive investment. In both panels, three model formulations are shown: resource-budget only (RB, blue), additive weather cue (RB+WC, orange), and interactive weather cue (RB×WC, green). All continuous model outputs are scaled to a common left axis for visualisation; reference seed counts are shown on the secondary right axis.

Over the multi-year period (Figure 3B), simulated time series revealed that mast years emerge from the interaction between gradual resource accumulation and episodic depletion associated with reproductive investment. High seed production years coincided with strong reductions in the resource budget, followed by one or more recovery years during which carbon reserves were replenished. Conversely, low-seeding years were associated with incomplete resource recovery or unfavourable climatic conditions limiting reproductive allocation. Environmental veto processes were also

reproduced: adverse conditions during flowering or seed development reduced realised seed production despite prior resource allocation, and the carbon initially committed to reproduction was partially returned to the internal resource pool, dampening interannual variability in resource depletion. The three model formulations diverged in their multi-year reproductive dynamics (Figure 3B). The resource-budget-only formulation (RB) produced relatively stable resource trajectories, with seed production varying primarily with accumulated carbon and showing limited interannual contrast. Incorporating temperature cues (RB+WC and RB×WC) introduced greater variability, with mast years becoming more episodic and more tightly coupled to lagged climatic signals. In the interactive formulation (RB×WC), cue sensitivity was modulated by internal resource status, so that favourable temperature conditions triggered strong reproductive responses only when carbon reserves were sufficient. These coupled endogenous and exogenous processes generated the characteristic boom–bust cycles of mast seeding observed in European beech and provide the mechanistic foundation for the model performance evaluation presented in the following sections.

3.2. Simulating mast seeding in beech

Model performance increased with the inclusion of weather cues and was highest when cue effects depended on internal resource status. At the tree-year scale (Figure 4), explained variance increased from $R^2 = 0.34$ in the resource-budget-only formulation (RB) to $R^2 = 0.44$ in the additive cue model (RB + WC) and $R^2 = 0.58$ in the interactive model (RB×WC). The RB formulation reproduced only a compressed version of the observed dynamics: simulated seed production remained relatively high even when observed values approached zero, whereas high-seeding years were systematically underestimated. Incorporating weather cues improved the separation between low- and high-seeding years, yielding steeper fitted relationships and predictions closer to the 1:1 expectation. This effect was strongest in the interactive formulation (RB×WC), indicating that responses to favourable weather cues are better captured when modulated by internal resource status.

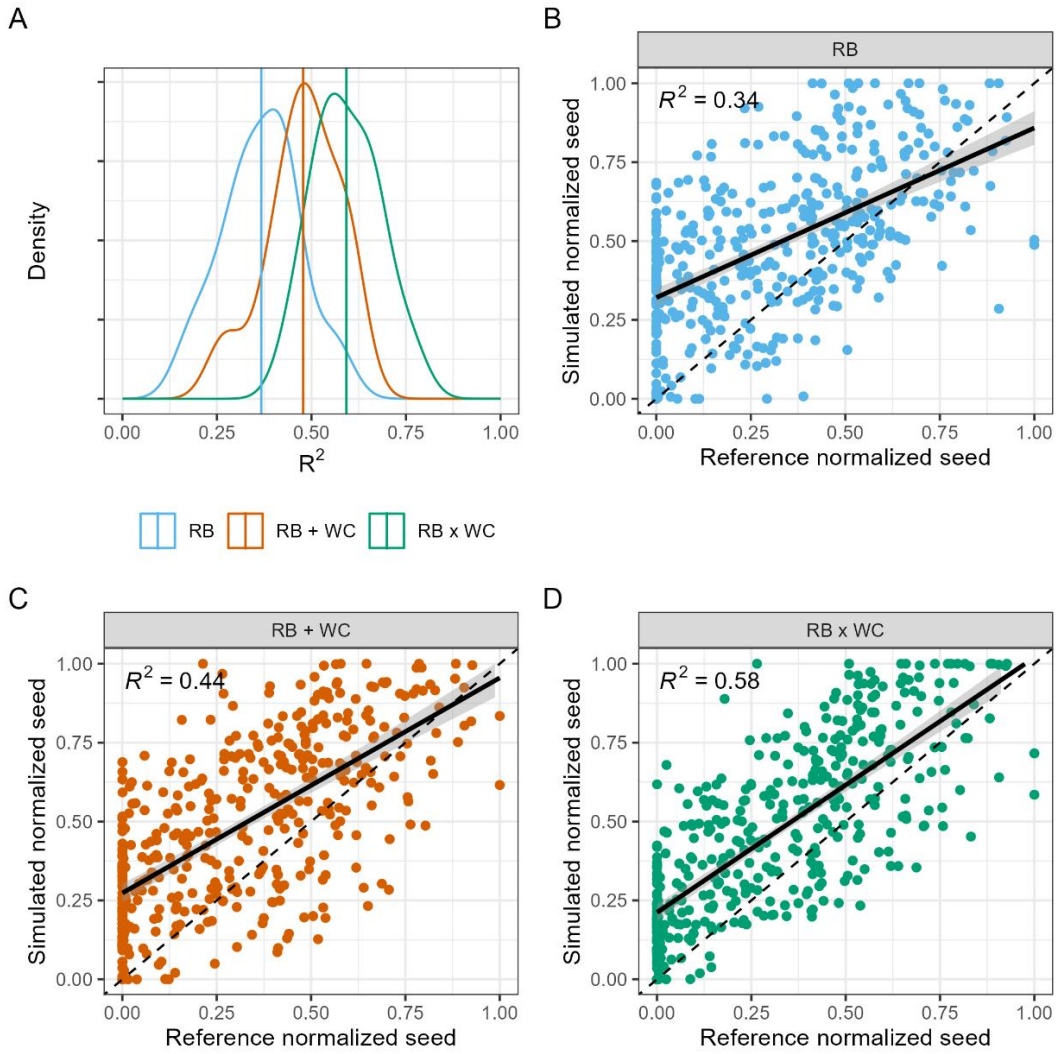

Figure 4. Model performance across alternative formulations of reproductive allocation across tree-years. (A) Distribution of model performance (R^2) for the three model formulations: resource budget only (RB; blue), resource budget with additive weather cues (RB+WC; orange), and resource budget with interactive weather cues (RB×WC; green). Vertical lines indicate median values for each formulation. (B-D) Relationship between observed (reference) and simulated normalised seed production for each model formulation: (B) RB, (C) RB+WC, and (D) RB×WC. Points represent mean normalised annual site observations, solid lines show fitted linear regressions, and shaded bands indicate 95% confidence intervals. The dashed 1:1 line denotes perfect agreement between observed and simulated values. Reported R^2 values quantify the proportion of variance explained by each model.

After aggregating prediction to the site-year level (Figure 5), model performance improved across all formulations, with R^2 raising from 0.58 (RB) to 0.64 (RB+WC) and 0.76 (RB×WC). All formulations performed better at the site-year level than at the tree-year scale, suggesting that part of the mismatch at finer resolution reflects among-tree variability that is averaged out at coarser spatial scales. The same ranking among formulations was retained after aggregation, with RB×WC providing the closest match to the observed range and the strongest discrimination between low- and high-seeding years (Figure 5C).

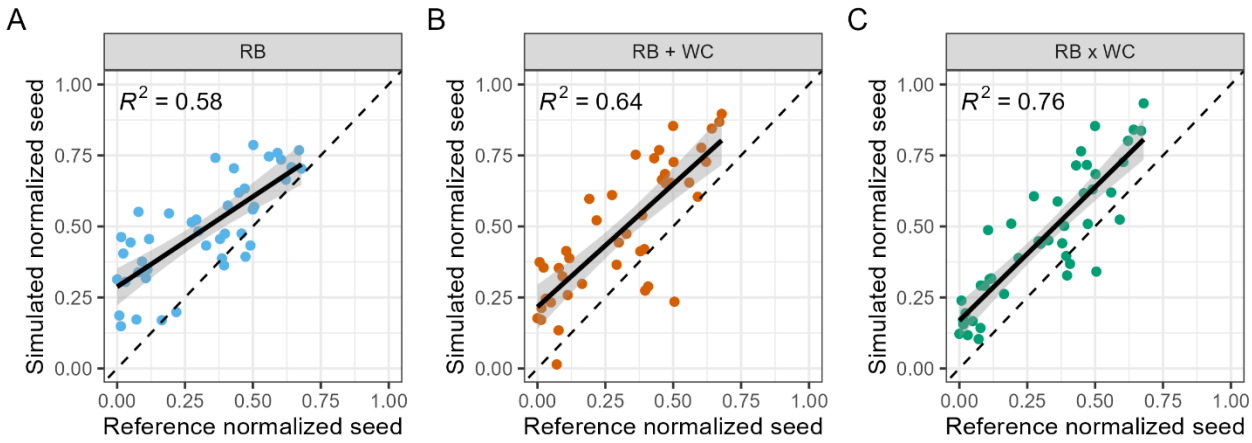

Figure 5. Model performance across alternative formulations of reproductive allocation, across site-years. Relationship between observed (reference) and simulated normalised seed production for each model formulation: resource budget only (RB; A), resource budget with additive weather cues (RB+WC; B), and resource budget with interactive weather cues (RB×WC; C). Points represent mean normalised annual site-year observations, solid lines show fitted linear regressions, and shaded bands indicate 95% confidence intervals. The dashed 1:1 line denotes perfect agreement between observed and simulated values. Reported R^2 values quantify the proportion of variance explained by each model. Timeseries of observed and simulated data are presented in Figure S3.

Model performance was quite robust to the choice of parameterisation strategy. Under domain-wide calibration, where a single parameter set was estimated jointly across all 11 sites, the RB×WC formulation retained most of its predictive skill, with site-level R^2 values ranging from 0.39 to 0.58, compared to 0.45–0.75 under site-specific calibration (Figure S5). The reduction in performance was modest and consistent across sites, suggesting that the model captures processes that are largely transferable across the UK beech network rather than site-idiosyncratic responses.

Figure 6 illustrates how model formulations differ in the relationships between resource level, weather cues, and seed production. In the RB formulation, simulated seed production changed only weakly along the weather-cue gradient (Figure 6A). Because weather cues do not enter the reproductive allocation rule in this formulation, this shallow positive trend should not be interpreted as a direct cue effect. Instead, it likely arises because the seasonal conditions captured by the cue metric also covary with carbon gain and thus with the resource budget available for reproduction. Consistently, the RB heatmap is structured mainly along the budget axis, with limited variation across the cue axis (Figure 6B). The cue-informed formulations differed in how weather and resources combined to determine seed output. In RB+WC, seed production increased with both budget level and cue strength, consistent with an additive contribution of the two drivers. In RB×WC, the effect of weather cues depended on internal resource status: favourable cues had a stronger effect when budgets were high, whereas low budgets constrained seed production even under strong cues (Figure 6A, B).

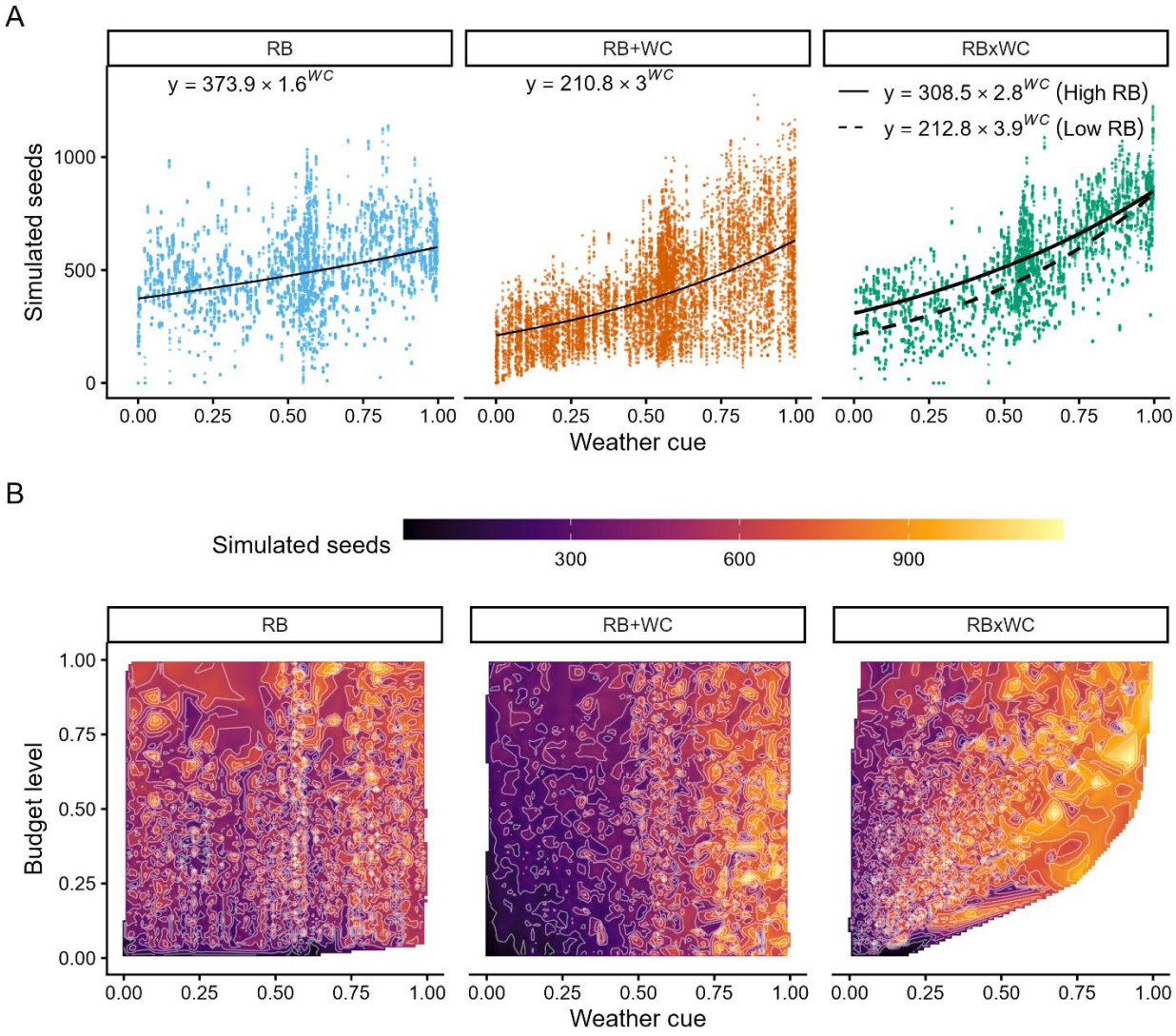

Figure 6. Joint effects of resource budget and weather cues on simulated seed production. (A) Relationship between weather cue and simulated seed production across model formulations. Points represent individual simulations, and lines show fitted exponential functions. In the interactive formulation (RB×WC), separate curves are shown for high (solid line) and low (dashed line) resource budget levels, illustrating how sensitivity to weather cues depends on internal resource status. (B) Heatmaps of mean simulated seed production across the two-dimensional state space defined by weather cue (x-axis) and resource budget level (y-axis). Colours range from dark (low) to light (high seed production). In the RB model, seed production depends primarily on resource availability, whereas in RB+WC it increases with both drivers independently. In RB×WC, high seed output is concentrated in the upper-right region of the state space, where both resource levels and weather cues are high, reflecting the multiplicative interaction between internal state and environmental forcing.

3.3. Modelling masting under climate change

Observed interannual variation in seed production remained high from the 1980–1990 to the 2000–2005 window and then declined sharply, with CVp peaking at approximately 1.22 around 2005

and decreasing to about 0.72 in the 2020–2025 window (Figure 7A). All three model formulations underestimated the absolute magnitude of interannual variability throughout the time series, with simulated CVp consistently below observed values by approximately 0.5–0.6 units across all windows. They nonetheless reproduced part of the temporal structure, with agreement between simulated and observed CVp improving markedly with model complexity (Figure 7B-D).

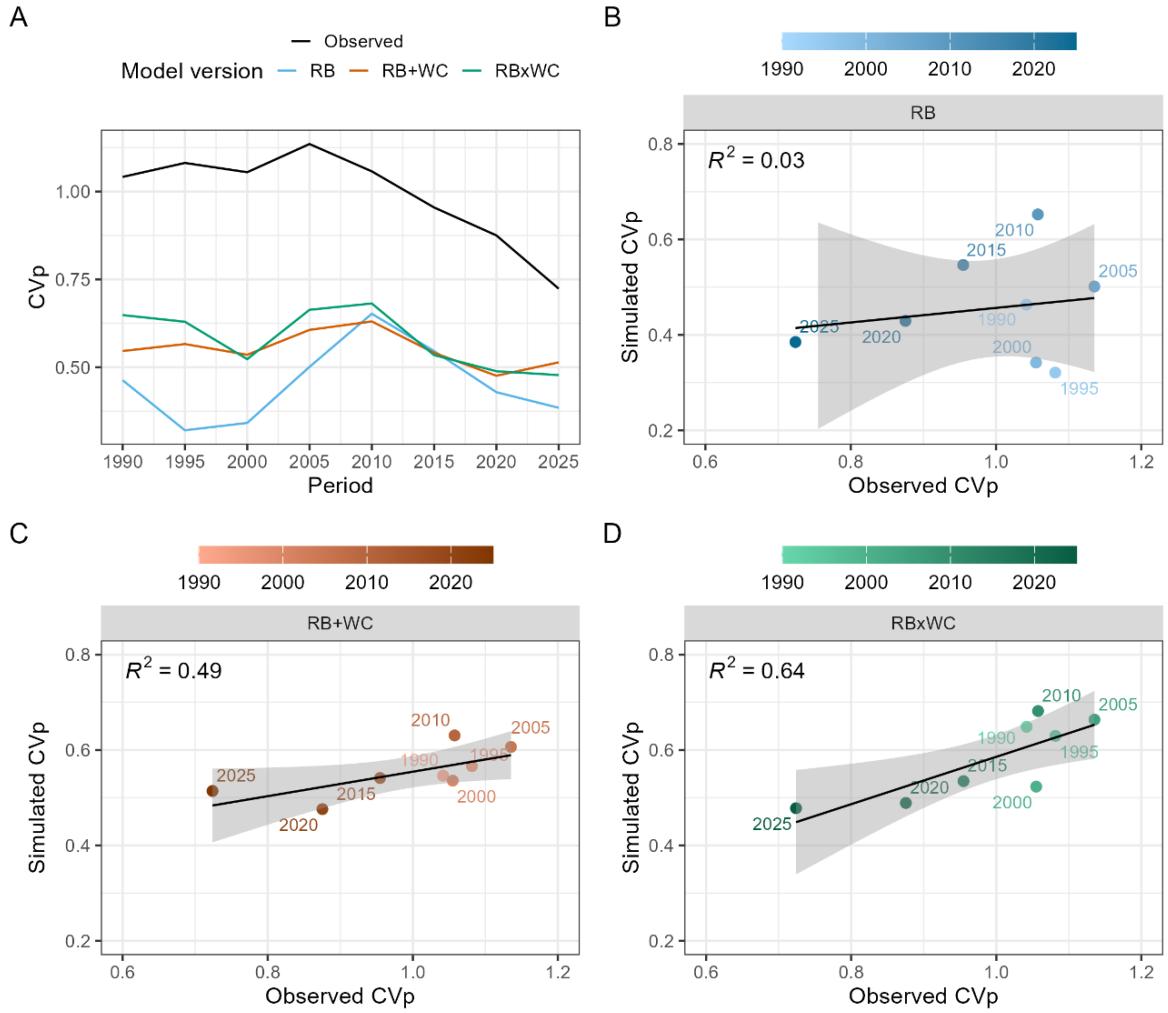

Figure 7. Temporal dynamics of masting intensity across model formulations. (A) Observed and simulated changes in masting intensity (interannual variation in seed production, CVp) over time in UK beech populations. The black line shows observed dynamics; coloured lines represent simulations for resource budget only (RB; blue), resource budget with additive weather cues (RB+WC; orange), and resource budget with interacting weather cues (RB×WC; green). CVp is calculated using 10-year moving windows with a step-size of 5 years; values are reported as the final year of each window (e.g., 1990 corresponds to 1980–1990). (B–D) Relationship between observed and simulated CVp across time windows for each model formulation: RB (B), RB+WC (C), and RB×WC (D). Point color indicates the time window, ranging from light (earlier periods) to dark (more recent periods). Solid lines show fitted linear regressions with 95% confidence intervals. Trends in the proportion of reproductive failures are shown in Figure S6.

The RB formulation showed virtually no correspondence with observed temporal dynamics (R^2 = 0.03), with simulated CVp varying independently of observed values across time windows. Simulated values ranged from ~0.33 (1995) to ~0.62 (2010), remaining well below the observed range (~1.08–1.22) throughout the series, and showing a partial recovery after 1995 that has no clear counterpart in the observations. The additive formulation (RB+WC) captured a larger share of the temporal variance (R^2 = 0.49), with simulated CVp ranging from ~0.55 to ~0.63 and correctly ranking many windows in terms of relative masting intensity, though still substantially underestimating the observed magnitude. The interactive formulation (RB×WC) showed the strongest agreement (R^2 = 0.64), with simulated CVp ranging from ~0.50 to ~0.65 and the temporal sequence of windows more consistently reflected. Earlier high-intensity windows (around 2005–2010) were correctly associated with higher simulated CVp (~0.65), and more recent windows (2020–2025) with lower values (~0.50).

3.4. Application: forecasting

We used the RB×WC model to forecast site-level seed production for 2023–2025, with all calibrations based exclusively on 1980–2022 observational data (Figure 8).

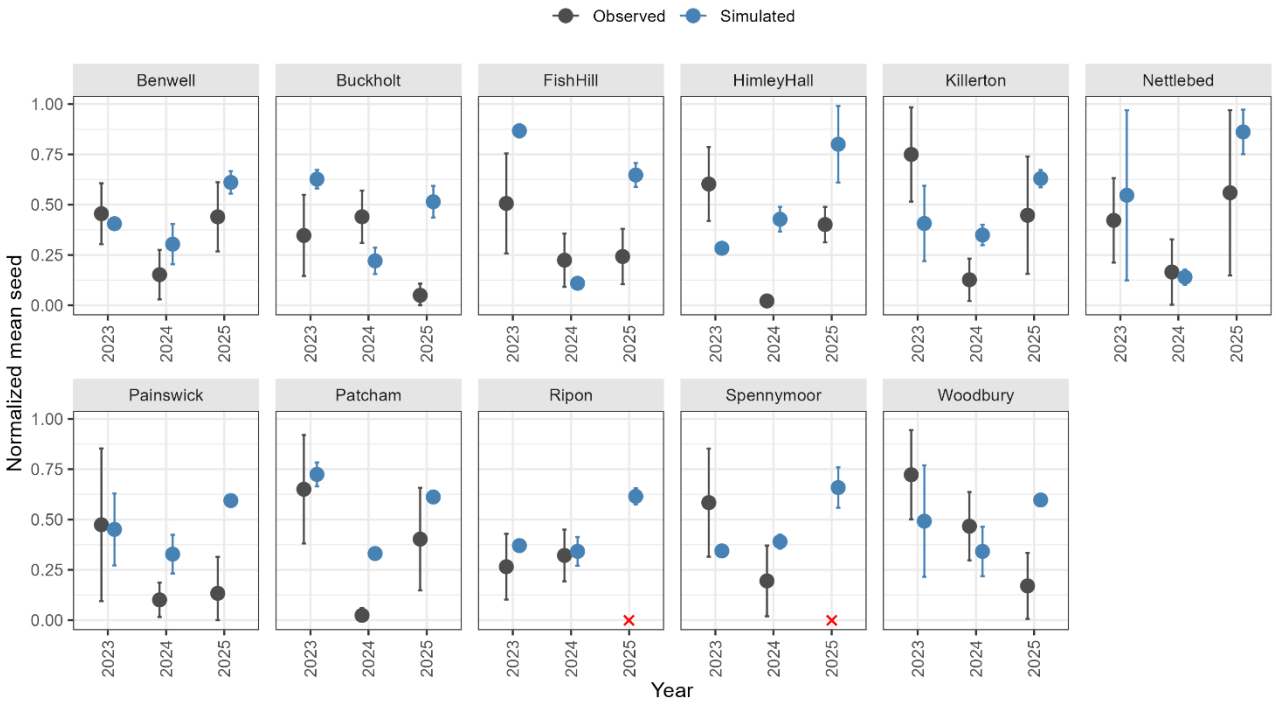

Figure 8. Site-level forecasts of normalised seed production for 2023–2025. Observed (grey) and simulated (blue) normalised seed production across UK beech sites, generated using the RB×WC model calibrated on 1980–2022 data. Points represent mean normalised seed production per site and year; vertical lines indicate among-tree variability. The 2025 observation was unavailable for Ripon and Spennymoor (×).

Forecast accuracy varied among sites and years. The 2023 crop was generally well

reproduced, with simulated values close to observations at most sites. The 2024 low-production year was captured at several sites including Benwell, Killerton, and Nettlebed, where the model correctly predicted below-average seed output. However, the 2025 crop was systematically overestimated: at sites where observed production remained low or moderate (e.g., Buckholt, Painswick, Patcham, Woodbury, HimleyHall, FishHill), simulated values were substantially higher than observations. This pattern suggests that the model does not fully capture the persistence of low-production conditions across consecutive years, possibly reflecting limitations in how the resource budget recovers after repeated low-seed years. Observations for 2025 were unavailable for Ripon and Spennymoor at the time of writing.

4. Discussion

Our study shows that a process-based model integrating resource dynamics and weather cues can reproduce key features of masting in European beech. Weather cues were necessary to match observed site-level dynamics, whereas the resource-budget-only formulation performed substantially worse. Model performance improved consistently with formulation complexity, both at the tree-year scale (R^2 = 0.34 for RB, 0.44 for RB+WC, 0.58 for RB×WC; Figure 4) and after aggregating to the site-year scale (R^2 = 0.58, 0.64 and 0.76, respectively; Figure 5). This confirms that weather cues improved model fit and that this improvement was strongest when cue sensitivity depended on internal resource status. The consistent ranking across spatial scales supports the idea that favourable weather cues trigger strong reproduction only when trees have sufficient stored resources (Monks *et al.*, 2016; Kelly *et al.*, 2025). Model performance was asymmetric, with high-seeding years reproduced more closely than low-seeding (failure) years. This is an improvement over earlier forecasting models that struggled at both ends of the distribution (Journé *et al.*, 2023), but also an indication that the mechanisms producing very low seed crops remain incompletely represented (Oberklammer *et al.*, 2026). The temporal analysis of interannual variability (CVp) showed that agreement between simulated and observed CVp across time windows improved markedly with model complexity, from RB (R^2 = 0.03) to RB+WC (R^2 = 0.49) and RB×WC (R^2 = 0.64; Figure 7), indicating that the interactive formulation successfully captured the relative ranking of high- and low-variability periods. However, all formulations systematically underestimated the absolute magnitude of CVp throughout the series and underestimated the sustained long-term decline in masting intensity observed after 2005, suggesting that the effects of increasingly frequent cue years on resource depletion and recovery are not yet fully represented. The 2023-2025 forecasts show that the model captures broad short-term variation in seed production among sites and years, but the underestimation of the long-term decline in masting intensity may partly explain the weaker forecasting performance

in recent years. MASTHING provides a useful tool for hypothesis testing and near-term forecasting, while clearly indicating where further refinement is needed for long-term prediction.

The contrast between the resource-only model formulation and the cue-informed models clarifies how different processes contribute to masting dynamics. Resource dynamics alone generated interannual variation in seed production, but they produced too few zero-seed years and failed to align reproduction with the observed timing of mast and failure years. Thus, fluctuations in resource acquisition by themselves were not sufficient to reproduce the empirical masting patterns, consistent with the notion that resource matching alone cannot explain mast years (Kelly, 1994; Pearse *et al.*, 2016). At the same time, even in the RB-only model, seed production showed a shallow positive relationship with weather cue strength (exponential base = 1.6; Figure 6A), despite the absence of an explicit cue effect. In our model, this relationship emerges because warmer summers enhance photosynthesis and resource accumulation, not because temperature acts as a flowering cue. This is interesting as it suggests a plausible starting point for the evolutionary argument proposed by Janzen (Janzen, 1971, 1976): hypersensitivity to weather cues may build on a pre-existing physiological sensitivity of reproduction to weather variation, which selection then amplifies into a stronger, cue-driven response. That interpretation is consistent with the idea that selective amplification acts on initially modest synchrony among individuals responding to the same environmental signal, eventually producing stronger interannual variation and synchrony (Bogdziewicz *et al.*, 2020b). Adding weather cues steepened the response substantially (base = 3.0 in RB+WC; Figure 6A), improving the temporal correspondence between simulations and observations, and this improvement was strongest when cue sensitivity depended on internal resource status: in the RB×WC formulation, trees with high resource budgets showed a steeper response to cues (base = 2.8) than those with low budgets (base = 3.9 on the low-budget curve, but starting from a lower intercept), producing the strongly nonlinear surface visible in Figure 6B. Under that formulation, mast and failure years were more often reproduced in the correct years, and high-seeding years were captured more closely. This suggests that resource-dependent cue sensitivity captures an important component of reproductive timing that was missing from earlier forecasting models (Journé *et al.*, 2023).

The observed decline in interannual variation in seed production in the UK, and more broadly across the beech range (Foest *et al.*, 2024; 2025; Jantzen *et al.*, 2026), was captured only partially across model formulations, with the RB×WC formulation reproducing the sustained downward trend most closely. Observed CVp peaked at approximately 1.22 around 2005 and declined to ~0.72 by 2025. Simulated formulations remained within a narrower range (~0.38–0.65), but the RBxWC formulation was able to track the sustained decrease (Figure 7D). Empirical analyses attribute this breakdown to increasing summer temperatures, which increase the frequency of flowering cues

(Bogdziewicz *et al.*, 2021). More frequent cues are thought to shorten recovery intervals between large seed crops, leading to progressive resource depletion and, in turn, weaker responses to subsequent cues (Hacket-Pain *et al.*, 2025). Our simulations are consistent with this mechanism in relative terms: under the RB×WC formulation, increased cue frequency generated a long-term decline in variability, indicating that the model can recover the directional breakdown in masting intensity. At the same time, the magnitude of this decline remained weaker than observed. Resource budgets fluctuated, but they did not decline through time enough to reduce reproductive responsiveness to the extent seen in the empirical record. This likely reflects the current allocation scheme, in which reproductive investment increases smoothly with cue strength and resource level, remains bounded, and is constrained by available reserves, while annual carbon gain allows partial recovery. These features buffer the system against chronic depletion, dampening the progressive weakening of masting intensity that is observed empirically. Notably, while the RB×WC formulation successfully ranked time windows by their relative variability ($R^2 = 0.64$ across periods; Figure 8B–D), it still underestimated CVp by approximately 0.5–0.6 units throughout the series, indicating that the model captures the temporal ordering of high- and low-variability periods and the overall decline through time, but not their absolute magnitude. The results suggest that the model underestimates the strength of depletion feedbacks needed to reproduce the observed breakdown in masting quantitatively. One additional potential improvement would be to replace the current sigmoidal cue response with a steeper, potentially exponential function, so that repeated warm summers generate stronger reproductive drawdown and more pronounced resource depletion (Fernández-Martínez *et al.*, 2017). MASTHING now provides a mechanistic platform for testing alternative hypotheses about how increasing cue frequency, resource depletion, and carry-over effects interact to drive the climate-related breakdown of masting.

The model also showed useful short-term forecasting ability. When calibrated with data from 1980-2022 and projected forward, it reproduced broad year-to-year variation in seed production during 2023-2025, as well as some of the among-site differences in crop size. At the same time, performance was uneven: seed production was generally overestimated in 2024 and 2025, especially at sites where the observed crop was low or intermediate. Thus, the model captures broad variation in seed production better than it predicts the exact magnitude. This pattern likely reflects the same limitation identified in the long-term CVp analysis the model's resource budget recovers too readily after reproductive events, preventing the carry-over depletion that may sustain low-production conditions in consecutive years. Thus, the model captures broad interannual variation in seed production better than it predicts the exact magnitude of low or consecutive poor crops, a pattern consistent with the broader challenge in mast forecasting of predicting extreme outcomes (Journé *et*

517 *al.*, 2023; Wion *et al.*, 2025). Even so, such forecasts can have clear operational value (Pearse *et al.*,
518 2021; Oberklammer *et al.*, 2026). Anticipating relatively productive years can support seed
519 collection, nursery planning, staff allocation, and storage preparation, and also adaptively set game
520 management and hunting bags for pulsed-resource consumers (Bisi *et al.*, 2018), while identifying
521 likely poor years may help avoid unnecessary financial and organisational investment. MASTHING
522 therefore already provides a useful forecasting framework, even if further refinement is needed to
523 improve prediction of low seed crops and local departures from observed seed production.
524 Beyond predictive performance, MASTHING provides a conceptual advance over purely
525 statistical approaches by explicitly tracking the physiological pathways linking weather, phenology,
526 carbon balance, and reproduction. Because the model resolves resource dynamics at daily resolution,
527 it can be used to test the contribution of specific mechanisms by modifying cue functions or activating
528 and suppressing heat, cold, and drought effects. The comparison among model formulations
529 presented here is itself an example of this hypothesis-testing capacity: the contrasting response
530 surfaces in Figure 6 directly illustrate how alternative assumptions about resource–cue coupling
531 translate into different predictions, and the CVp analysis (Figure 7) identifies the specific aspect of
532 masting dynamics, i.e., the long-term decline in interannual variability, that current formulations fail
533 to capture and that future refinements should target. A particular strength of the framework is the
534 coupling of reproduction to canopy phenology, which controls the seasonal timing of carbon
535 acquisition and reproductive decisions. In the current implementation, weather cues are evaluated
536 within a fixed post-solstice window (Journé *et al.*, 2024), but the model structure would also allow
537 cue perception to be linked directly to phenological development. Such an extension could improve
538 the representation of state-dependent cue expression, potentially helping to explain both extreme
539 mast years and the long-term changes in masting intensity documented here and elsewhere (Foest *et*
540 *al.*, 2024, 2025; Jantzen *et al.*, 2026). Because the model is relatively parsimonious in its input
541 requirements and can be transferred through parameter recalibration, MASTHING also provides a
542 flexible framework for extending this approach to other masting species, allowing cross-species tests
543 of whether the same resource–cue coupling mechanisms underlie masting across taxa.
544 To summarise, we developed MASTHING, a process-based model that integrates phenology-
545 driven resource acquisition, a dynamic resource budget, temperature-based flowering cues, and
546 environmental vetoes during pollination and seed ripening. The model reproduced key features of
547 European beech masting across multiple scales, especially the timing of mast and failure years and
548 short-term site-level variation in seed production, with highest performance when cue sensitivity
549 depended on internal resource status (Kelly *et al.*, 2025). At the same time, low-seeding years were
550 less well captured than high-seeding years, and the 2025 crop was systematically overestimated

across sites. Although the model reproduced the observed long-term decline in masting intensity, it underestimated its magnitude, as the CVp analysis showed that simulated trajectories remained less variable than the observed series despite correctly ranking high- and low-variability periods. These mismatches point to specific processes that require refinement, particularly the strength of resource depletion feedbacks and the shape of the cue-response function under increasing cue frequency. Nonetheless, the results show that a process-based framework can translate current mechanistic understanding into both insight on long-term change and useful short-term forecasts, provide a platform for testing alternative hypotheses about resource–climate coupling, and identify the specific limitations that must be addressed to improve the quantitative accuracy of long-term prediction of masting dynamics under climate change.

Acknowledgements

This study was funded by the Italian Ministry of Agriculture, Food Sovereignty and Forestry (MASAF, SOFIA, DM 0656382), by Ferrero Trading Lux (HAZIMUT project) and by the European Union (ERC, ForestFuture, 101039066). Views and opinions expressed are, however, those of the authors only and do not necessarily reflect those of the European Union or the European Research Council. Neither the European Union nor the granting authority can be held responsible for them. AI tools (Claude, Chat-GPT) were used to improve the clarity and readability of portions of this manuscript. All scientific content, analyses, and interpretations remain entirely the work of the authors, who take full responsibility for the accuracy of the information presented.

Author Contributions Statement

All authors designed the study, SBr developed the model with input from FC, CF, SBa, AHP, MB. SBr, AHP, MB, and FC co-wrote the paper. All authors revised the text and approved the submission.

Declaration of interests

No competing interests to declare.

Data and code availability statement

The data that support the findings of this study are available from with the permission of dr. Andrew Hacket-Pain. Data requests should be addressed to andrew.hacket-pain@liverpool.ac.uk. The MASTHING source code is openly available at https://github.com/GeoModelLab/MASTHING and archived on Zenodo (https://doi.org/10.5281/zenodo.19660460). The MASTHING source code is

584 openly available at https://github.com/GeoModelLab/MASTHING and archived on Zenodo
585 (https://doi.org/10.5281/zenodo.19660460).
586
587 **References**

588 Asse, D., Randin, C.F., Bonhomme, M., Delestrade, A. & Chuine, I. (2020). Process-based models
589 outcompete correlative models in projecting spring phenology of trees in a future warmer climate.
590 Agricultural and Forest Meteorology, p. 107931.
591 Bajocco, S., Ricotta, C. & Bregaglio, S. (2025). Bridging the gap between remotely sensed phenology
592 and the underlying ecophysiological processes: The SWELL model. *Methods in Ecology and*
593 *Evolution*, 16, 1473–1488.
594 Bartelink, H.H. (1997). Allometric relationships for biomass and leaf area of beech (*Fagus sylvatica* L.).
595 *Annales des sciences forestières*, 54, 39–50.
596 Bisi, F., Chirichella, R., Chianucci, F., Von Hardenberg, J., Cutini, A., Martinoli, A. *et al.* (2018). Climate,
597 tree masting and spatial behaviour in wild boar (*Sus scrofa* L.): insight from a long-term study.
598 *Annals of Forest Science*, 75, 46.
599 Bogdziewicz, M., Steele, M., Marino, S. & Crone, E. (2018). Correlated seed failure as an environmental
600 veto to synchronize reproduction of masting plants. *New Phytologist*, 219.
601 Bogdziewicz, M., Ascoli, D., Hacket-Pain, A., Koenig, W.D., Pearse, I., Pesendorfer, M. *et al.* (2020a).
602 From theory to experiments for testing the proximate mechanisms of mast seeding: an agenda for
603 an experimental ecology. *Ecology Letters*.
604 Bogdziewicz, M., Kelly, D., Tanentzap, A.J., Thomas, P.A., Lageard, J.G. & Hacket-Pain, A. (2020b).
605 Climate change strengthens selection for mast seeding in European beech. *Current Biology*, 30, 3477–
606 3483.e2.
607 Bogdziewicz, M., Kelly, D., Thomas, P.A., Lageard, J.G.A. & Hacket-Pain, A. (2020c). Climate warming
608 disrupts mast seeding and its fitness benefits in European beech. *Nature Plants*, 6, 88–94.
609 Bogdziewicz, M., Hacket-Pain, A., Kelly, D., Thomas, P.A., Lageard, J. & Tanentzap, A.J. (2021).
610 Climate warming causes mast seeding to break down by reducing sensitivity to weather cues. *Global*
611 *Change Biology*, 27, 1952–1961.
612 Bogdziewicz, M., Kelly, D., Tanentzap, A.J., Thomas, P., Foest, J., Lageard, J. *et al.* (2023). Reproductive
613 collapse in European beech results from declining pollination efficiency in large trees. *Global*
614 *Change Biology*, 29, 4595–4604.
615 Bogdziewicz, M., Kelly, D., Ascoli, D., Caignard, T., Chianucci, F., Crone, E.E. *et al.* (2024). Evolutionary
616 ecology of masting: mechanisms, models, and climate change. *Trends in Ecology & Evolution*, 39,
617 851–862.

618 Bregaglio, S., Ginaldi, F., Raparelli, E., Fila, G. & Bajocco, S. (2023). Improving crop yield prediction
619 accuracy by embedding phenological heterogeneity into model parameter sets. *Agricultural Systems*,
620 209, 103666.
621 Bregaglio, S., Bajocco, S., Ferrara, C., Bogdziewicz, M., Hacket-Pain, A., & Chianucci, F. (2026).
622 MASTHING: a process-based model of mast seeding in European beech (Version 1.0.0) [Computer
623 software]. *Zenodo*. https://doi.org/10.5281/zenodo.19660460
624 Briscoe, N.J., Morris, S.D., Mathewson, P.D., Buckley, L.B., Jusup, M., Levy, O. *et al.* (2022).
625 Mechanistic forecasts of species responses to climate change: The promise of biophysical ecology.
626 *Global Change Biology*, 29, 1451–1470.
627 Clark, J.S., Nuñez, C.L. & Tomasek, B. (2019). Foodwebs based on unreliable foundations: spatiotemporal
628 masting merged with consumer movement, storage, and diet. *Ecological Monographs*, 89, e01381.
629 Crone, E.E. & Rapp, J.M. (2014). Resource depletion, pollen coupling, and the ecology of mast seeding.
630 *Annals of the New York Academy of Sciences*, 1322, 21–34.
631 Elliott, G. & Kemp, J. (2016). Large-scale pest control in New Zealand beech forests. *Ecological*
632 *Management and Restoration*, 17, 200–209.
633 Fernández-Martínez, M., Bogdziewicz, M., Espelta, J.M. & Peñuelas, J. (2017). Nature beyond linearity:
634 Meteorological variability and jensen's inequality can explain mast seeding behaviour. *Frontiers in*
635 *Ecology and Evolution*, 5.
636 Foest, J., Bogdziewicz, M., Ascoli, D., Pesendorfer, M., Cutini, A., Nussbaumer, A. *et al.* (2024).
637 Widespread breakdown in masting in European beech due to rising summer temperatures. *Global*
638 *Change Biology*, 30, e17307.
639 Foest, J.J., Szymkowiak, J., Dyderski, M.K., Jastrzębowski, S., Fuchs, H., Ratajczak, E. *et al.* (2025). No
640 refuge at the edge for European beech as climate warming disproportionately reduces masting at colder
641 margins. *Ecology Letters*, 28, e70284.
642 Hacket-Pain, A. & Bogdziewicz, M. (2021). Climate change and plant reproduction: trends and drivers
643 of mast seeding change. *Philosophical Transactions of the Royal Society B*, 376, 20200379.
644 Hacket-Pain, A., Szymkowiak, J., Journé, V., Barczyk, M.K., Thomas, P.A., Lageard, J.G.A. *et al.* (2025).
645 Growth decline in European beech associated with temperature-driven increase in reproductive
646 allocation. *Proceedings of the National Academy of Sciences*, 122.
647 Hirsch, M., Puhlmann, H., Klemmt, H.-J. & Seifert, T. (2025). Modelling fructification intensity at the
648 tree level reveals species-specific effects of tree age, social status and crown defoliation across major
649 European tree species. *European Journal of Forest Research*, 144, 1505–1522.
650 Holben, B.N. (1986). Characteristics of maximum-value composite images from temporal AVHRR data.
651 *International Journal of Remote Sensing*, 7, 1417–1434.

652 Hufkens, K. (2023). The MODISTools package: an interface to the MODIS Land Products Subsets Web
653 Services. doi:10.5281/zenodo.7551165, https://doi.org/10.5281/zenodo.7551165.
654 Isagi, Y., Sugimura, K., Sumida, A. & Ito, H. (1997). How does masting happen and synchronize?
655 *Journal of Theoretical Biology*, 187, 231–239.
656 Jantzen, C., Burant, J., Gamelon, M., Bakker, E.L. & Visser, M.E. (2026). Masting breakdown in European
657 beech reduces fitness benefits of masting, partly explained by climate change. Preprint
658 https://doi.org/10.32942/X2B95Q.
659 Janzen, D.H. (1971). Seed predation by animals. *Annual Review of Ecology and Systematics*, 220, 465–
660 492.
661 Janzen, D.H. (1976). Why bamboos wait so long to flower. *Annual Review of Ecology and Systematics*, 7,
662 347–391.
663 Journé, V., Hacket-Pain, A. & Bogdziewicz, M. (2023). Evolution of masting in plants is linked to
664 investment in low tissue mortality. *Nature Communications*, 14, 7998.
665 Journé, V., Hacket-Pain, A., Oberklammer, I., Pesendorfer, M.B. & Bogdziewicz, M. (2023). Forecasting
666 seed production in perennial plants: identifying challenges and charting a path forward. *New*
667 *Phytologist*, 239, 466–476.
668 Journé, V., Szymkowiak, J., Foest, J., Hacket-Pain, A., Kelly, D. & Bogdziewicz, M. (2024). Summer
669 solstice orchestrates the subcontinental-scale synchrony of mast seeding. *Nature Plants*, 10, 367–373.
670 Kabeya D, Iio A, Kakubari Y, Han Q. (2021). Dynamics of non-structural carbohydrates following a full
671 masting event reveal a role for stored starch in relation to reproduction in *Fagus crenata*. *Forest*
672 *Research (Fayettev)*, Oct 26, pp. 1–18.
673 Kelly, D. (1994). The evolutionary ecology of mast seeding. *Trends in Ecology Evolution*, 9, 465–470.
674 Kelly, D., Geldenhuis, A., James, A., Holland, E.P., Plank, M.J., Brockie, R.E. *et al.* (2013). Of mast and
675 mean: differential-temperature cue makes mast seeding insensitive to climate change. *Ecology Letters*,
676 16, 90–98.
677 Kelly, D., Hart, D.E. & Allen, R.B. (2001). Evaluating the wind pollination benefits of mast seeding.
678 *Ecology*, 82, 117–126.
679 Kelly, D. & Sork, V.L. (2002). Mast seeding in perennial plants: Why, how, where? *Annual Review of*
680 *Ecology and Systematics*, 33, 427–447.
681 Kelly, D., Szymkowiak, J., Hacket-Pain, A. & Bogdziewicz, M. (2025). Fine-tuning mast seeding: as
682 resources accumulate, plants become more sensitive to weather cues. *New Phytologist*, 246, 1975–
683 1985.

LaMontagne, J.M., Redmond, M.D., Wion, A.P. & Greene, D.F. (2021). An assessment of temporal variability in mast seeding of north american Pinaceae. *Philosophical Transactions of the Royal Society B: Biological Sciences*, 376, 20200373.

Lin, Y.S., Medlyn, B.E. & Ellsworth, D.S. (2012). Temperature responses of leaf net photosynthesis: the role of component processes. *Tree Physiology*, 32, 219–231.

Maselli, F., Chiesi, M., Angeli, L., Fibbi, L., Rapi, B., Romani, M. *et al.* (2020). An improved ndvi-based method to predict actual evapotranspiration of irrigated grasses and crops. *Agricultural Water Management*, 233, 106077.

Medlyn, B.E. (1998). Physiological basis of the light use efficiency mode. *Tree Physiolooy*, 18, 167–176.

Monks, A., Monks, J.M. & Tanentzap, A.J. (2016). Resource limitation underlying multiple masting models makes mast seeding sensitive to future climate change. *New Phytologist*, 210, 419–430.

Monteith, J.L. (1972). Solar radiation and productivity in tropical ecosystems. *Journal of Applied Ecology*, 9, 747–766.

Mäkelä, A., Landsberg, J., Ek, A.R., Burk, T.E., Ter-Mikaelian, M., Ågren, G.I. *et al.* (2000). Process-based models for forest ecosystem management: current state of the art and challenges for practical implementation. *Tree Physiology*, 20, 289–298.

Oberklammer, I., Gratzer, G., Schueler, S., Konrad, H., Hacket-Pain, A. & Pesenforfer, M.B. (2026). See(d)ing the seeds - toward weather-based forecasting of annual seed production in six European forest tree species. *EcoEvoRxiv*. https://doi.org/10.32942/X2T05Z

Ostfeld, R.S. & Keesing, F. (2000). Pulsed resources and community dynamics of consumers in terrestrial ecosystems. *Trends in Ecology Evolution*, 15, 232–237.

Packham, J.R., Thomas, P.A., Lageard, J.G. & Hilton, G.M. (2008a). The English beech masting survey 1980–2007: Variation in the fruiting of the common beech (*Fagus sylvatica* L.) and its effects on woodland ecosystems. *Arboricultural Journal*, 31, 189–214.

Packham, J.R., Thomas, P.A., Lageard, J.G.A. & Hilton, G.M. (2008b). The English beech masting survey 1980– 2007: Variation in the fruiting of the common beech (*Fagus sylvatica* L.) and its effects on woodland ecosystems. *Arboricultural Journal*, 31, 189–214.

Pearse, I.S., Koenig, W.D. & Kelly, D. (2016). Mechanisms of mast seeding: resources, weather, cues, and selection. *New Phytologist*, 212, 546–562.

Pearse, I.S., Wion, A.P., Gonzalez, A.D. & Pesendorfer, M.B. (2021). Understanding mast seeding for conservation and land management. *Philosophical Transactions of the Royal Society B: Biological Sciences*, 376, 34657466.

Rapp, J.M., Mcintire, E.J. & Crone, E.E. (2013). Sex allocation, pollen limitation and masting in whitebark pine. *Journal of Ecology*, 101, 1345–1352.

718 Roncé, I.L., Dardevet, E., Venner, S., Schönbeck, L., Gessler, A., Chuine, I. *et al.* (2023). Reproduction
719 alternation in trees: testing the resource depletion hypothesis using experimental fruit removal in
720 *Quercus ilex*. *Tree Physiology*, 43, 952–964.
721 Sala, A., Hopping, K., McIntire, E.J., Delzon, S. & Crone, E.E. (2012). Masting in whitebark pine (*Pinus*
722 *albicaulis*) depletes stored nutrients. *New Phytologist*, 196, 189–199.
723 Satake, A. & Journé, V. (2026). Linking gene regulation to flowering phenology under climate change: a
724 dynamical modelling approach. *Contemporary Physics*, 0, 1–11.
725 Shibata, M., Masaki, T., Yagihashi, T., Shimada, T. & Saitoh, T. (2020). Decadal changes in masting
726 behaviour of oak trees with rising temperature. *Journal of Ecology*, 108, 1088–1100.
727 Smaill, S.J., Clinton, P.W., Allen, R.B. & Davis, M.R. (2011). Climate cues and resources interact to
728 determine seed production by a masting species. *Journal of Ecology*, 99, 870–877.
729 Sofiev, M., Siljamo, P., Ranta, H., Linkosalo, T., Jaeger, S., Rasmussen, A. *et al.* (2013). A numerical
730 model of birch pollen emission and dispersion in the atmosphere. description of the emission module.
731 *International Journal of Biometeorology*, 57, 45–58.
732 Tattoni, C., Corradini, A., Chianucci, F., Ciolli, M., Giusti, R., Bragalanti, N. *et al.* (2025). Behaviour of
733 brown bears under fluctuating resource availability. *Ecology and Evolution*, 15, e71693.
734 Vacchiano, G., Ascoli, D., Berzaghi, F., Lucas-Borja, M.E., Caignard, T., Collalti, A. *et al.* (2018).
735 Reproducing reproduction: How to simulate mast seeding in forest models. *Ecological Modelling*,
736 376, 40–53.
737 Végh, L. & Kato, T. (2024). Modified seib-dgvm enables simulation of masting in a temperate forest.
738 *Ecological Modelling*, 488, 110577.
739 Végh, L. & Kato, T. (2024). Modified SEIB-DGVM enables simulation of masting in a temperate forest.
740 *Ecological* Modelling, 488, 110577.
741 Wion, A.P., Pearse, I.S., Broxson, M. & Redmond, M.D. (2025). Mast hindcasts reveal pervasive effects of
742 extreme drought on a foundational conifer species. *New Phytologist*, 246, 450–460.
743 Yeoh, S.H., Satake, A., Numata, S., Ichie, T., Lee, S.L., Basherudin, N. *et al.* (2017). Unravelling proximate
744 cues of mass flowering in the tropical forests of South-East Asia from gene expression analyses.
745 *Molecular Ecology*, 26, 5074–5085.
746 Zhao, C., Liu, B., Xiao, L., Hoogenboom, G., Boote, K.J., Kassie, B.T. *et al.* (2019). A simple crop
747 model. *European Journal of Agronomy*, 104, 97–106.
748 Zianis, D. & Mencuccini, M. (2004). On simplifying allometric analyses of forest biomass. *Forest*
749 *Ecology and Management*, 187, 311–332.

750 Zwolak, R., Celebias, P. & Bogdziewicz, M. (2022). Global patterns in the predator satiation effect of
751 masting: A meta-analysis. *Proceedings of the National Academy of Sciences of the United States*
752 *of America*, 119. e2105655119

753

Supplementary Information

S1. Full model description

MASTHING (MASting THeory modellING) is a process-based model that simulates mast seeding dynamics by coupling tree structure, phenology, carbon balance, environmental forcing, and reproductive allocation. The model operates at a daily time step and is driven by meteorological inputs (air temperature, precipitation, incoming radiation) together with tree structural attributes derived from diameter at breast height (DBH). At the core of the framework is a dynamic pool of mobile carbon reserves, hereafter referred to as the resource budget (B_t, g C m^{-2}), which integrates daily carbon gains from photosynthesis and losses due to maintenance respiration and reproductive allocation. All fluxes are expressed per unit crown projection area (CPA, m^2). Reproductive investment is represented as a continuous function of internal resource status and climatic cues, rather than a threshold-based switching mechanism, enabling evaluation of alternative hypotheses about resource-climate coupling.

S1.1. Allometric Initialisation

Tree structural properties are initialised from DBH (cm), the only required tree-level input. Crown projection area (CPA, m^2), tree height (H, m) and aboveground biomass components are derived from species-specific allometric relationships (Bartelink, 1997; Zianis & Mencuccini, 2004):

$$CPA = 0.4064 \times DBH^{1.2830} \quad \text{(SE1.1)}$$

$$H = exp(1.4192 + 0.5358 \times ln(DBH)) \quad \text{(SE1.2)}$$

$$ln(B_{tot}) = -1.3816 + 2.3485 \times ln(DBH) \quad \text{(SE1.3)}$$

$$ln(B_{stem}) = -1.6015 + 2.3427 \times ln(DBH) \quad \text{(SE1.4)}$$

$$ln(B_{branch}) = -5.2898 + 2.9353 \times ln(DBH) \quad \text{(SE1.5)}$$

$$B_f = 0.0001663 \times DBH^2 \times H + 0.224 \quad \text{(SE1.6)}$$

$$LA = 3.38 \times CPA\text{^}1.028 \quad \text{(SE1.7)}$$

$$LAI_{max} = (B_f \times SLA) / CPA \quad \text{(SE1.8)}$$

where B_{tot} (kg DM) is total aboveground biomass, B_{stem} and B_{branch} (kg DM) are stem and branch biomass, B_f (kg DM) is foliage biomass, LA (m^2) is total leaf area, LAI_{max} is maximum leaf area index, and SLA (m^2 kg^{-1}) is species-specific leaf area (Table S1.6). This formulation links biomass allocation directly to canopy structure, ensuring consistency between structural variables and photosynthetic capacity.

S1.2. Carbon Balance Module

Daily carbon dynamics are computed as the balance between gross primary production (GPP, g C m^{-2} d^{-1}) and maintenance respiration. GPP is estimated using a light-use efficiency approach:

$GPP_t = \varepsilon \times GSR_t \times 0.5 \times f_{int} \times f_T \times f_{stress}$ (SE1.9)

where ε is light use efficiency (g C MJ^{-1}), GSR_t is global solar radiation (MJ m^{-2} d^{-1}), 0.5 is the PAR fraction, $f_{int} = 1 - \exp(-0.5 \times LAI)$ is the canopy interception fraction, fT is a temperature response function (Yan & Hunt, 1999), and $f_{stress} = \min(f_{heat}, f_{cold}, f_{water})$ is the most limiting abiotic stress factor. The temperature response of photosynthesis follows the asymmetric function of Yan & Hunt (1999), which returns zero below a minimum ($T_{min,gro}$, °C) and above a maximum ($T_{max,gro}$, °C) temperature threshold:

$f_T = 0$, if $T_{avg} \leq T_{min,gro}$ or $T_{avg} \geq T_{max,gro}$ (SE1.10a)

$f_T = [(T_{max,gro} - T_{avg})/(T_{max,gro} - T_{opt,gro})] \times [(T_{avg} - T_{min,gro})/(T_{opt,gro} - T_{min,gro})]^{\alpha}$ otherwise (SE1.10b)

where $T_{avg} = (T_{max} + T_{min}) / 2$ is mean daily air temperature (°C), T_{opt}, is the optimum temperatures for growth (°C), and the exponent α controls the asymmetry of the response:

$\alpha = (T_{opt} - T_{min,gro}) / (T_{max,gro} - T_{opt})$ (SE1.10c)

The function rises from zero at $T_{min,gro}$, reaches a maximum of 1.0 at T_{opt}, and returns to zero at $T_{max,gro}$. Maintenance respiration is computed separately for woody (stem + branches; $R_{wood,t}$, g C m^{-2} d^{-1}) and foliar ($R_{leaf,t}$, g C m^{-2} d^{-1}) components using a Q_{10} formulation:

$R_{wood,t} = r_w \times Q_{10}^{(Tavg - 25)/10} \times (B_{stem} + B_{branch}) \times 0.5 \times 1000 / CPA$ (SE1.11a)

$R_{leaf,t} = r_l \times Q_{10}^{(Tavg - 25)/10} \times B_{foliage} \times (LAI / LAI_{max}) \times 1000 / CPA$ (SE1.11b)

where r_w and r_l are base respiration rates for wood and leaves respectively (g C g^{-1} DM d^{-1}), and T_{avg} is mean daily air temperature (°C). The factor 0.5 accounts for the carbon content of dry biomass.

Heat stress reduces photosynthesis when daily maximum temperature (T_{max}, °C) exceeds the growth maximum temperature ($T_{max,gro}$, °C). The response is a logistic sigmoid transitioning to zero at the critical heat temperature ($T_{crit,heat}$, °C):

$m_{heat} = (T_{max,gro} + T_{crit,heat}) / 2$ (SE1.12a)

$w_{heat} = T_{crit,heat} - T_{max,gro}$ (SE1.12b)

$f_{heat} = 1 / (1 + \exp(10 / w_{heat} \times (T_{max} - m_{heat})))$ (SE1.12c)

where $f_{heat} = 1$ when $T_{max} < T_{max,gro}$ (no stress) and $f_{heat} \rightarrow 0$ as T_{max} approaches $T_{crit,heat}$.

Cold stress reduces photosynthesis when daily minimum temperature (T_{min}, °C) falls below the growth minimum temperature ($T_{min,gro}$, °C). The transition occurs between the critical cold temperature ($T_{crit,cold}$, °C) and $T_{min,gro}$:

$m_{cold} = (T_{min,gro} + T_{crit,cold}) / 2$ (SE1.13a)

$w_{cold} = T_{min,gro} - T_{crit,cold}$ (SE1.13b)

$f_{cold} = 1 / (1 + \exp(10 / (-w_{cold}) \times (T_{min} - m_{cold})))$ (SE1.13c)

where $f_{cold} = 1$ when $T_{min} > T_{min,gro}$ and f_cold = 0 when $T_{min} \leq T_{crit,cold}$.

Reference evapotranspiration (ET_0, mm d^{-1}) is computed using the Hargreaves method:

$$ET_0 = (1/\lambda) \times 0.0023 \times ((T_{max} + T_{min})/2 + 17.8) \times (T_{max} - T_{min})^{0.5} \times R_a \quad \text{(SE1.14)}$$

where λ is the latent heat of vaporization (MJ kg^{-1}), and R_a is extraterrestrial radiation (MJ m^{-2} d^{-1}) computed from site latitude and day of year. A water availability index is then derived from the cumulative balance of ET_0 and precipitation (P, mm) over a moving window of 30 days (WS_{days}):

$$I = (\sum ET_0 - \sum P) / (\sum ET_0 + \sum P + \varepsilon) \quad \text{(SE1.15a)}$$

$$W_{avail} = 1 - (I + 1) / 2 \quad \text{(SE1.15b)}$$

where $\varepsilon = 10^{-6}$ is a small constant for numerical stability, $I \in [-1, +1]$, and $W_{avail} \in [0, 1]$ (0 = maximum drought, 1 = no stress). The water stress multiplier for GPP is then:

$$f_{water} = 0.5 \times (W_{avail} - W_{thresh}) + 1, \quad if\ W_{avail} < W_{thresh} \quad \text{(SE1.15c)}$$

$$f_{water} = 1, \quad if\ W_{avail} \geq W_{thresh} \quad \text{(SE1.15d)}$$

where W_{thresh} is the water stress threshold parameter.

The resource budget evolves daily as:

$$B_t = \max(0, B_{t-1} + GPP_t - R_{tree,t}) \quad \text{(SE1.16)}$$

where B_t (g C m^{-2}) is the resource budget at day t, GPP_t is gross primary production, and $R_{tree,t} = R_{wood,t} + R_{leaf,t}$ is total maintenance respiration. The maximum resource budget (B_{max}, g C m^{-2}) is set as a fixed fraction of total aboveground biomass:

$$B_{max} = f_B \times B_{tot} \quad \text{(SE1.17)}$$

where f_B is the resource budget fraction (calibrated; Table S1.6), a calibrated parameter controlling the size of the mobile carbon pool relative to structural biomass. The minimum budget required to initiate reproduction (B_{min}, g C m^{-2}) is defined as a threshold fraction of B_{max}:

$$B_{min} = \theta \times B_{max} \quad \text{(SE1.18)}$$

where θ is the reproduction threshold (calibrated; Table S1.6). The budget is initialised at the midpoint of the feasible range:

$$B_0 = (B_{min} + B_{max}) \times 0.5 \quad \text{(SE1.19)}$$

At the end of each growing season (31 December), the budget is normalised to a dimensionless budget level (BL) serving as the internal state variable for reproductive allocation (Section S1.4):

$$BL_t = (B_t - B_{min}) / (B_{max} - B_{min}), \quad BL_t \in [0, 1] \quad \text{(SE1.20)}$$

S1.3 Phenological Module

Tree phenology is simulated using the process-based SWELL model, which tracks dormancy induction, endodormancy, ecodormancy, growth, greendown, and senescence phases through photothermal accumulation. Phenological progression controls the seasonal window of carbon acquisition and the timing of reproductive decisions. A full description is provided in Bajocco et al. (2025). The growing season (phenoCode 3–5) determines the period over which GPP_t is computed and LAI scales with canopy development: LAI increases linearly with growth completion during leaf

expansion and declines proportionally to NDVI during senescence. The onset of flowering is triggered when growth completion reaches the parameter Flo_{time} (expressed as a percentage of the full growth forcing requirement, Table S1.6).

S1.4 Reproductive Allocation

Annual reproductive investment is determined by the combined effects of internal resource status and post-solstice temperature cues, incorporating both current-year and lagged climatic signals. Temperature cues are derived from mean daily maximum temperature during the post-solstice sensing window ($T_{sol,y}$, DOY 172–212). Cues from the current year (Y−1 relative to seed production, activating signal) and the preceding year (Y−2, inhibitory signal) are incorporated, reflecting the lagged structure typical of masting systems (Journé et al., 2024). Each signal is transformed through a sigmoid response function:

$$g_T(T, BL) = BL / (1 + \exp(\sigma \times s_T \times (T_{sol,y} - T_{mid}))) \quad \text{(SE1.21)}$$

where $\sigma = -1$ for the activating signal (warm summers promote reproduction) and $\sigma = +1$ for the inhibitory signal, s_T controls sensitivity (Table S1.6), and T_{mid} is the midpoint of the cue temperature range (°C). The midpoint T_{mid} and the temperature range of the cue function are not fixed a priori but are derived from the site-specific meteorological record. For each site, the mean post-solstice maximum temperature is computed annually:

$$T_{sol,y} = \text{mean}(T_{max,d}) \text{ for } d \in [172, 212] \text{ in year Y} \quad \text{(SE1.22a)}$$

The cue temperature range is then defined as:

$$T_{min,cue} = \min(T_{sol,y}) \text{ over all years} \quad \text{(SE1.22b)}$$

$$T_{max,cue} = \max(T_{sol,y}) \text{ over all years} \quad \text{(SE1.22c)}$$

$$T_{mid} = (T_{min,cue} + T_{max,cue}) / 2 \quad \text{(SE1.22d)}$$

This data-driven scaling ensures that the sigmoid response spans the full range of climatic variability observed at each site, so that the normalised cue signal reflects relative rather than absolute temperature anomalies. As a result, T_{mid} and the cue range are site-specific quantities computed from the historical meteorological record rather than calibrated parameters. In the RB+WC formulation BL = 1, so cues act independently of resource status; in RB×WC, BL is the actual normalised budget level, modulating cue sensitivity by internal resource status. The final weather cue is a weighted combination of the two years' signals:

$$TC_t = w_T \times g_T(T_{Y-1}, BL) + (1 - w_T) \times g_T(T_{Y-2}, BL) \quad \text{(SE1.23)}$$

where w_T is the weight assigned to the current-year signal (Table S1.6). Reproductive potential (RP) emerges as a continuous function of resource availability and climatic forcing:

$$RP_t = BL_t \quad \text{(RB formulation)} \quad \text{(SE1.24a)}$$

$$RP_t = (BL_t + TC_t) / 2 \quad \text{(RB+WC, RB×WC formulations)} \quad \text{(SE1.24b)}$$

Reproductive investment (I_{rep}, g C m^{-2}) is computed as the minimum of available reserves and potential investment, and partitioned between flowering and fruit development:

$$I_{rep} = \min(B_t, RP_t \times B_{max}) \quad \text{(SE1.25a)}$$

$$I_{seed} = I_{rep} / (1 + c_{ff}) \quad \text{(SE1.25b)}$$

$$I_{flow} = I_{rep} - I_{seed} \quad \text{(SE1.25c)}$$

where c_{ff} is the flowers-to-fruit cost (Table S1.6), the additional carbon cost of flower production relative to seed ripening. Realised reproduction is further reduced by unfavourable conditions during flowering and seed development. Pollination efficiency is computed as a sigmoidal function of daily precipitation during the flowering window ($Flo_{time} \pm Flo_{duration}$ /2):

$$f_{poll} = 1 / (1 + \exp(k \times (P_{day} - P_{mid}))) \quad \text{(SE1.26)}$$

where $P_{mid} = P_{lim}$ / 2, P_{lim} is the precipitation threshold limiting pollination (Table 1.6) and k is a sensitivity term derived from P_{lim}. High precipitation during anthesis reduces pollination efficiency, scaling down flowering and ripening investment proportionally. During the greendown phase, seed ripening progresses following a logistic function of greendown completion ($GD\%$, %), modulated by water stress:

$$f_{rip} = 1 / (1 + \exp(-k_r \times (GD\% - 50))) \quad \text{(SE1.27)}$$

where $k_r = 0.09$ is a fixed parameter controlling the steepness of the ripening response. Resources saved by incomplete ripening under drought stress are returned to the budget. After reproduction, the remaining resource budget is carried over to the following year:

$$B_{t+1,init} = B_t - I_{rep} + R_{veto} \quad \text{(SE1.28)}$$

where R_{veto} (g C m^{-2} d^{-1}) represents resources recovered from incomplete seed ripening. This carry-over links past reproductive investment to future carbon availability, generating the interannual feedbacks characteristic of masting systems.

S1.5 Model formulations

Three alternative formulations of reproductive allocation were evaluated. In the RB formulation, reproduction depends exclusively on internal reserves ($RP_t = BL_t$; SE1.24a), and temperature cues do not enter the allocation rule. In the RB+WC formulation, cues contribute additively to reproductive potential (SE1.24b) but act independently of resource status ($BL = 1$ in SE1.21), so warm post-solstice temperatures promote reproduction regardless of current reserves. In the RB×WC formulation, cue sensitivity is explicitly modulated by the normalised budget level ($BL = BL_t$ in SE1.21), so favourable cues amplify reproduction only when reserves are sufficient. These three formulations represent alternative hypotheses about resource–climate coupling and are compared against the same observational dataset (Section 2.2).

S1.6 Model Parameters

Table S1.6. Key parameters of the MASTHING model for *Fagus sylvatica*.

Module	Parameter	Symbol	Value	Source
Allometry	CPA coefficient	—	0.4064	Literature
	CPA exponent	—	1.2830	Literature
	Height intercept (ln)	—	1.4192	Literature
	Height slope	—	0.5358	Literature
	Biomass intercept (ln)	—	−1.3816	Literature
	Biomass slope	—	2.3485	Literature
	Specific leaf area	SLA	23	Literature
Carbon balance	Light use efficiency	ε	3.0 g C MJ^{-1}	Literature
	Min. growth temperature	$T_{min,gro}$	3.5 °C	Literature
	Opt. growth temperature	T_{opt}	18.0 °C	Literature
	Max. growth temperature	$T_{max,gro}$	30.0 °C	Literature
	Critical heat temperature	$T_{crit,heat}$	38.0 °C	Literature
	Critical cold temperature	$T_{crit,cold}$	1.0 °C	Literature
	Wood respiration rate	r_w	3×10^{-5} g C g^{-1} DM d^{-1}	Literature
	Leaf respiration rate	r_l	2×10^{-4} g C g^{-1} DM d^{-1}	Literature
	Q_{10} coefficient	Q_{10}	1.8	Literature
	Water stress memory	—	30 days	Literature
	Water stress threshold	W_{thresh}	0.5	Literature
	Resource budget fraction	f_B	Calibrated	—
	Reproduction threshold	θ	Calibrated	—
	Initial budget fraction	—	$0.5 \times (B_{min} + B_{max})$	Derived
Reproduction	Flowering time	Flo_{time}	5	Fixed
	Flowering duration	$Flo_{duration}$	12 % growth completion	Fixed
	Pollination precip. threshold	P_{lim}	Calibrated	—
	Flower-to-fruit cost	c_{ff}	0.14	Fixed
	Cue sensitivity	s_T	2.8	Fixed
	Current-year cue weight	w_T	Calibrated	—
	Cue temperature midpoint	T_{mid}	Site-specific (SE1.22)	Derived
	Cue temperature range	$T_{min,cue} - T_{max,cue}$	Site-specific (SE1.22b–c)	Derived
	Ripening steepness	k_r	0.09	Fixed

Parameters estimated through optimisation are indicated as 'Calibrated'; fixed parameters derived from literature or ecophysiological constraints are indicated accordingly.

S2. Resource-modulated temperature cue functions

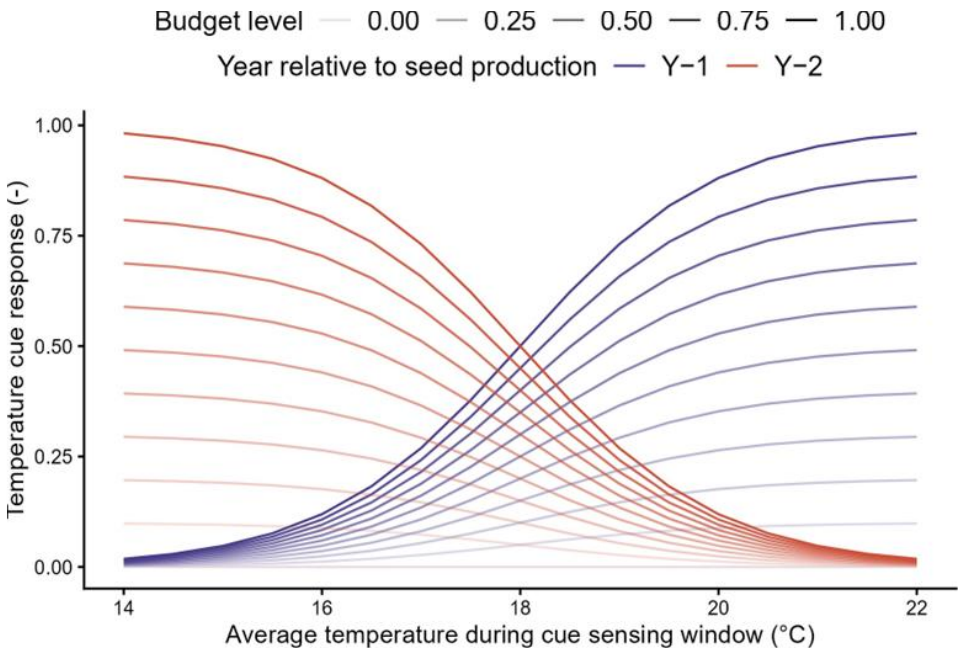

Figure S2. Resource-modulated temperature cue functions controlling reproductive investment. The curves represent theoretical sigmoidal relationships illustrating how temperature cues in year Y-1 (blue, activating effect) and year Y-2 (red, inhibitory legacy effect) contribute to reproductive investment as a function of average temperature during the cue-sensing window. Each set of curves represents different levels of resource availability (budget level, ranging from 0 to 1), with line transparency decreasing as resource availability declines. The y-axis shows the scaled cue response (0–1). Higher resource availability amplifies the magnitude of both activating and inhibitory responses, whereas low resource levels dampen their effects. These functions are not fitted to empirical data but represent assumptions built into the model to capture the expected nonlinear sensitivity of reproductive timing to thermal conditions.

S3. Study sites overview

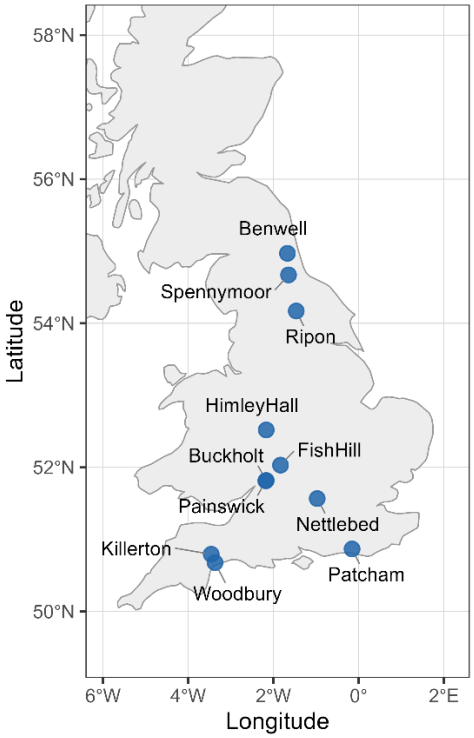

Site	N trees	First yr	Last yr	N obs
Benwell	10	1983	2025	343
Spennymoor	10	1981	2024	318
Ripon	15	1981	2024	469
HimleyHall	11	1980	2025	260
FishHill	14	1981	2025	267
Buckholt	14	1980	2025	455
Painswick	6	1980	2025	187
Nettlebed	13	1981	2025	308
Patcham	10	1980	2025	272
Killerton	11	1980	2025	309
Woodbury	15	1980	2025	409

Figure S3. Geographic distribution and characteristics of the 11 UK beech study sites. Left panel: site locations across England. Right panel: site-level summary statistics including number of monitored trees (after excluding trees with fewer than 10 years of observations), observation period, and total number of seed production records

S4. Time series of observed and simulated data for the three model versions

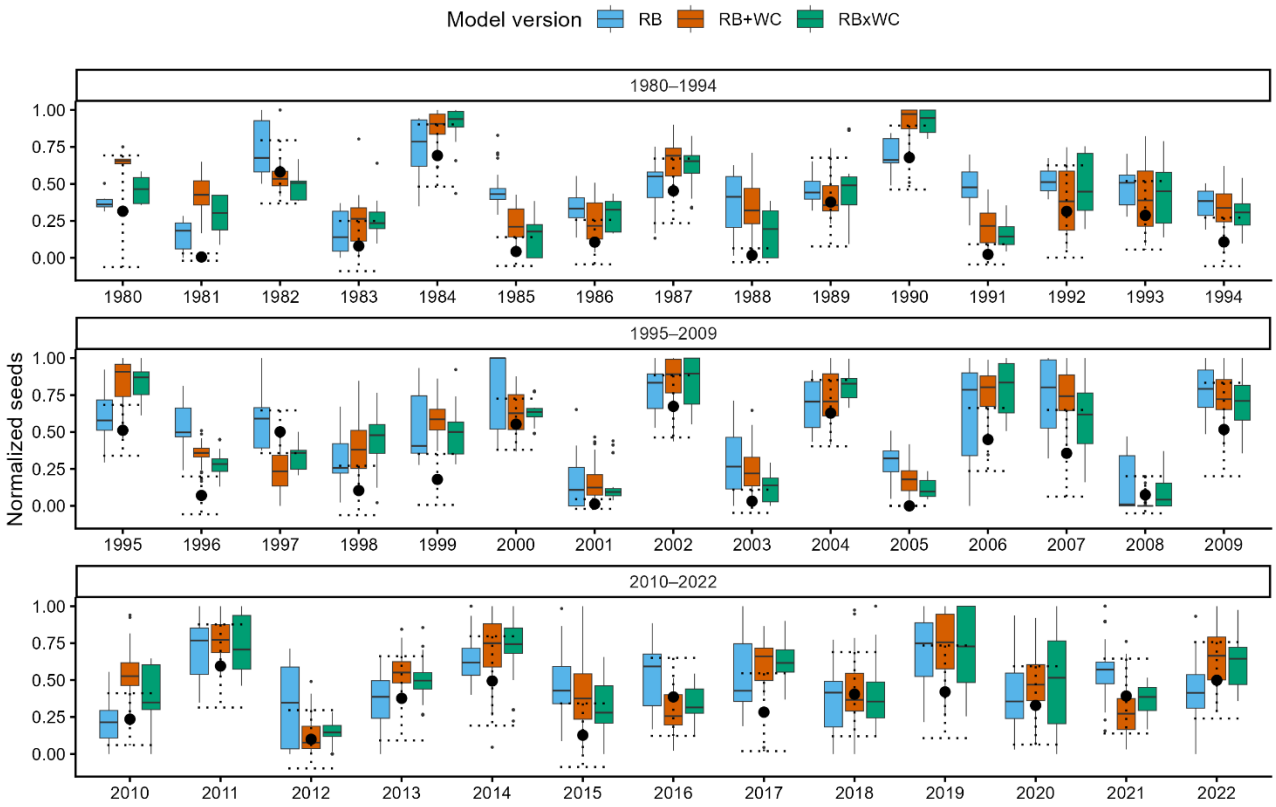

Figure S4. Time series of observed and simulated normalised seed production across model formulations. Each panel covers a sub-period of the calibration window (1980–1994, 1995–2009, 2010–2022). For each year, boxplots show the distribution of simulated normalised seed production across trees and sites for the three model formulations: resource budget only (RB; blue), resource budget with additive weather cues (RB+WC; orange), and resource budget with interactive weather cues (RB×WC; green). Boxes span the interquartile range, horizontal lines indicate the median, whiskers extend to 1.5× the interquartile range, and dots indicate outliers. Filled circles show the mean observed normalised seed production across sites for each year.

Simulated and observed normalised seed production are compared annually across the full calibration period in Figure S4. All three formulations reproduce the broad interannual structure of the observed time series, with mast years (e.g., 1992, 2002, 2014, 2019) generally associated with higher simulated values and failure years (e.g., 1995, 2001, 2012) with lower ones. The RB formulation tends to produce narrower distributions and less extreme low values, consistent with the absence of a direct cue mechanism. The cue-informed formulations (RB+WC and RB×WC) show greater year-to-year variability and more frequent alignment between simulated distributions and observed values, particularly in mast years. Across all formulations, low-production years are less well captured than high-production years, with observed near-zero values often falling below the lower tail of the simulated distribution.

S5. Site-level model performance under site-specific and domain-wide parameterisation

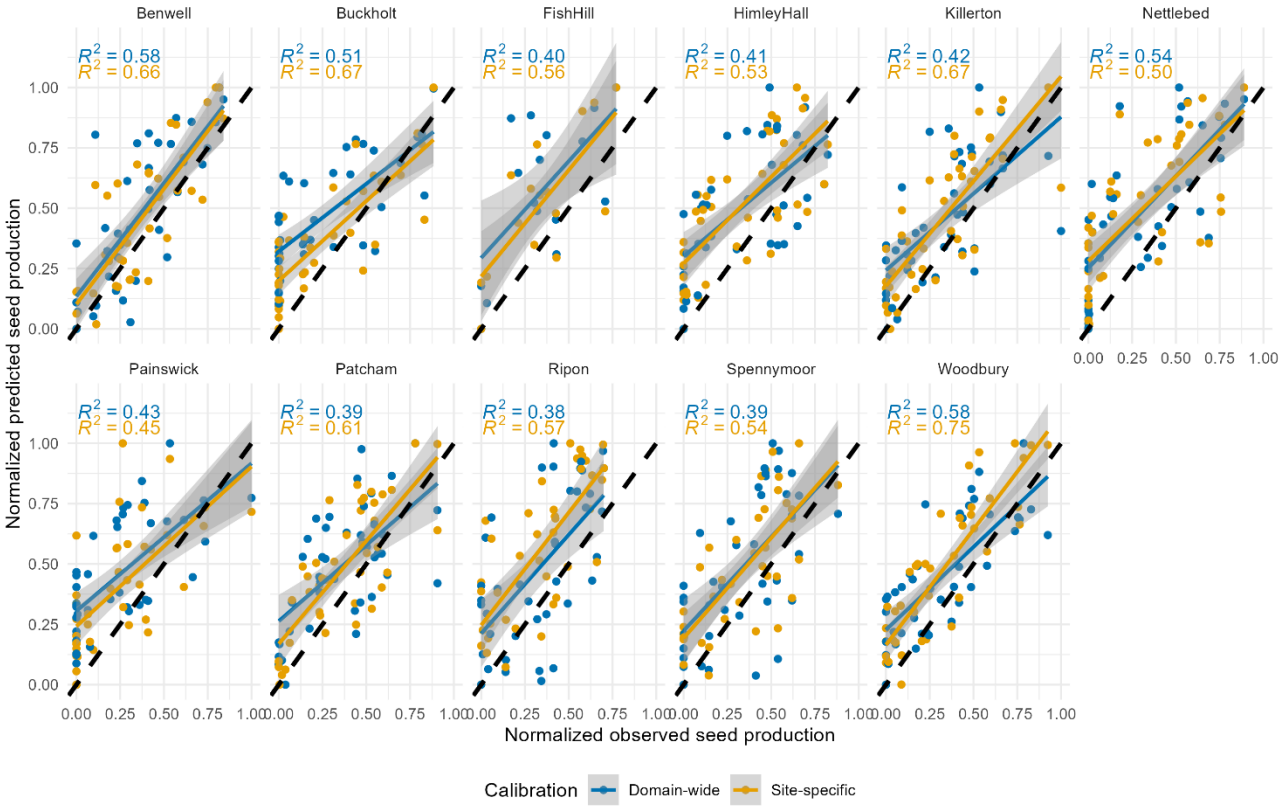

Figure S5. Site-level model performance under site-specific and domain-wide parameterisation strategies for the RB×WC formulation. Each panel shows the relationship between observed and simulated normalised seed production at a single site, with separate regression lines for site-specific (orange) and domain-wide (blue) calibration. R^2 values are reported for each strategy. The dashed 1:1 line denotes perfect agreement. Domain-wide calibration uses a single parameter set estimated jointly across all sites; site-specific calibration optimises parameters independently per site.

Model performance was robust to the choice of parameterisation strategy. Under domain-wide calibration — where a single parameter set was estimated jointly across all 11 sites — the RB×WC formulation retained most of its predictive skill, with site-level R^2 values ranging from 0.39 to 0.58, compared to 0.45–0.75 under site-specific calibration (Figure S5). The reduction in performance was modest and consistent across sites, suggesting that the model captures processes that are largely transferable across the UK beech network rather than site-idiosyncratic responses. This result supports the use of domain-wide parameterisation for operational forecasting at unsampled locations.

S6. Temporal dynamics of reproductive failure across model formulations

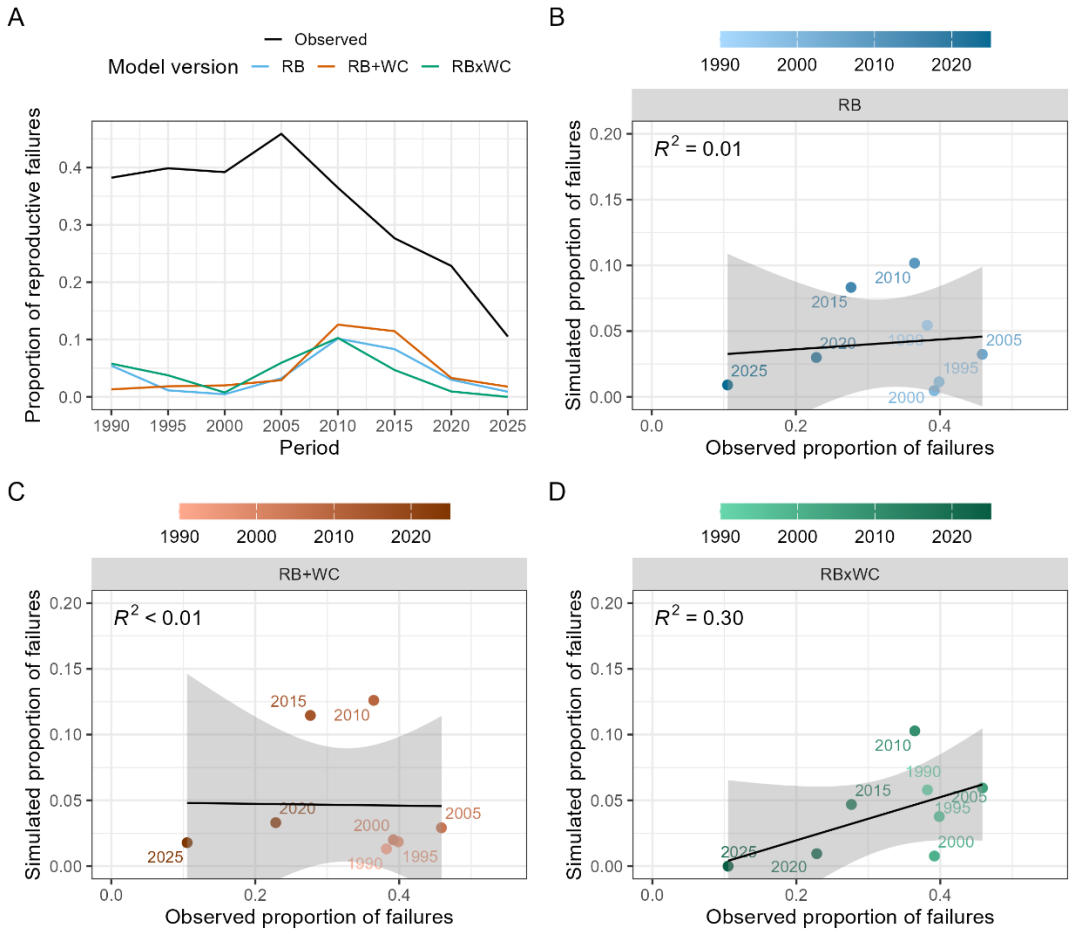

Figure S6. (A) Observed and simulated proportion of reproductive failure years (defined as normalised seed production < 0.05) computed over 10-year moving windows with a 5-year step, reported as the final year of each window (e.g., 1990 corresponds to 1980–1990). The black line shows observed dynamics; coloured lines show simulations for RB (blue), RB+WC (orange), and RB×WC (green). (B–D) Relationship between observed and simulated failure proportions across time windows for each model formulation. Point color indicates the time window, ranging from light (earlier periods) to dark (more recent periods). Solid lines show fitted linear regressions with 95% confidence intervals.

The proportion of reproductive failure years declined substantially over the study period, from approximately 0.39 around 1990 to 0.11 by 2025 (Figure S6A). All three model formulations underestimated failure frequency throughout the series, with simulated values remaining below 0.13 across all periods and all formulations, well below the observed range. Agreement between simulated and observed failure proportions across time windows was poor for RB ($R^2 = 0.01$) and RB+WC ($R^2 < 0.01$), with both formulations showing no meaningful correspondence with the temporal ordering of observed failure rates. The RB×WC formulation showed modest but non-trivial improvement ($R^2 = 0.30$; Figure S6D), correctly associating more recent low-failure periods with lower simulated failure frequencies, though it still failed to reproduce the magnitude of the observed decline. These results are consistent with the CVp analysis and confirm that the long-term reduction in reproductive variability, including both the weakening of interannual variation and the decline in failure frequency, is not captured by any of the current model formulations.